Transition Metal Nanocluster Formation Kinetic and Mechanistic Studies. A New Mechanism When Hydrogen Is the Reductant: Slow, Continuous Nucleation and Fast Autocatalytic Surface Growth

Murielle A. Watzky and Richard G. Finke*

Contribution from the Department of Chemistry, Colorado State University, Fort Collins, Colorado 80523

Received February 18, 1997[⊗]

Abstract: Following an overview of the primitive state of mechanistic studies of the formation of nanoclusters, with a focus on LaMer's classic work on the formation of sulfur sols, kinetic and mechanistic studies of the formation of our recently reported novel $P_2W_{15}Nb_3O_{62}^{9-}$ polyoxoanion- and Bu_4N^+- stabilized $Ir_{\sim 190-450}$ (hereafter, $Ir(0)_{\sim 300}$) nanoclusters are presented. The work reported consists of the full experimental and other details of the following eight major components: (i) development of an indirect—but easy, continuous, highly quantitative and thus powerful—method to monitor the formation of the Ir(0) nanoclusters via their catalytic hydrogenation activity and through the concept of pseudoelementary reaction steps; (ii) application of the appropriate kinetic equations for nucleation and autocatalysis, and then demonstration that these equations fit the observed, sigmoidal-shaped kinetic curves *quantitatively* with resultant rate constants k_1 and k_2; (iii) confirmation by a more direct, GLC method that the method in (i) indeed works and does so quantitatively, yielding the same k_1 and k_2 values within experimental error; (iv) collection of a wealth of previously unavailable kinetic and mechanistic data on the effects on nanocluster formation of added olefin, H_2 pressure, anionic nanocluster stabilizer ($[Bu_4N]_9P_2W_{15}Nb_3O_{62}$ in the present case), H_2O, HOAc, and temperature; (v) careful consideration and ruling out of other hypotheses, notably that particle-size rate effects *alone* might account for the observed sigmoidal shaped curves; and then (vi) distillation of the results into a minimalistic mechanism consisting of several pseudoelementary steps. Also presented as part of the Discussion are (vii) a concise but comprehensive review of the literature of transition metal nanocluster formation under H_2 as the reducing agent, an analysis which provides highly suggestive evidence that the new mechanism uncovered is a much more general mechanism—if not a new paradigm—for transition metal nanoclusters formed under H_2 (and, the data argue, probably also for related reducing agents); and (viii) a summary of the seven key predictions of this new mechanism which remain to be tested (four predictions are the expected predominance of magic-number size nanoclusters; designed control of nanocluster size via the living-metal polymer concept; the synthesis of onion-skin structure bi-, tri-, and higher-metallic nanoclusters; and the use of face-selective capping agents as a way to block the autocatalytic surface growth and, thereby, to provide designed-shape nanoclusters). Overall, it is hoped that the results—the first new mechanism in more than 45 years for transition metal nanocluster formation—will go far toward providing a firmer mechanistic basis, and perhaps even a new paradigm, for the designed synthesis of new transition metal nanoclusters of prechosen sizes, shapes, and mono- to multimetallic compositions.

Introduction

There is an enormous interest presently in nanoparticles[1] (<10 nm, i.e., <100 Å)[2], especially in the synthesis of near-monodisperse (i.e., ≤±15%)[2] nanoclusters where their size, size-distribution, composition and shape are controlled via *designed syntheses*. Even though metal colloids (>10 nm)[2] have been known since the time of Faraday,[3] and even though important advances towards the above synthetic objectives are beginning to appear,[4] it is still not possible presently to design successful syntheses of a prechosen nanocluster. Indeed and to the

[⊗] Abstract published in *Advance ACS Abstracts,* October 1, 1997.

(1) Reviews on nanoclusters: (a) Jena, P.; Rao B. K.; Khanna, S. N. *Physics and Chemistry of Small Clusters*; Plenum: New York, 1987. (b) Andres, R. P.; Averback, R. S.; Brown, W. L.; Brus, L. E. Goddard, W. A.; Kaldor, A.; Louie S. G.; Moscovits, M.; Peercy, P. S.; Riley, S. J.; Siegel, R. W.; Spaepen, F.; Wang, Y. *J. Mater. Res.* **1989**, *4*, 704. This is a Panel Report from the United States Department of Energy, Council on Materials Science on Research Opportunities on Clusters and Cluster-assembled Materials. (c) Thomas, J. M. *Pure Appl. Chem.* **1988**, *60*, 1517. (d) Henglein, A. *Chem. Rev.* **1989**, *89*, 1861. (e) A superb series of papers, complete with a record of the insightful comments by the experts attending the conference, is available in *Faraday Discussions* **1991**, *92*, 1−300. (f) Bradley, J. S. In *Clusters and Colloids. From Theory to Applications*; Schmid, G., Ed.; VCH: New York, 1994; pp 459−544. (g) Schmid, G. In *Aspects of Homogeneous Catalysis*; Ugo, R., Ed.; Kluwer: Dordrecht, 1990; Chapter 1. (h) Bönnemann, H.; Braun, G.; Brijoux, W.; Brinkmann, R.; Tilling, A. S.; Seevogel, K.; Siepen, K. *J. Org. Met. Chem.* **1996**, *520*, 143−162 and the collection of "key publications" cited as refs 2−61 therein.

(2) (a) See elsewhere for a review of nanocluster catalysis which includes necessary key terms and definitions of[2b] nanoclusters; traditional colloids; monodisperse and near-monodisperse nanoparticles; "magic number" (i.e., full shell and thus enhanced stability) nanoclusters; Schwartz's updated definition of homogeneous vs heterogeneous catalysts; inorganic ("charge") and organic ("steric") stabilization mechanisms for colloids and nanoparticles; plus a review of the Bu_4N^+ and polyoxoanion-stabilized $Ir(0)_{\sim 300}$ nanoclusters discussed herein. (b) Aiken, J. D., III; Lin, Y.; Finke, R. G. *J. Mol. Catal.* **1996**, *114*, 29−51.

(3) Faraday, M. *Phil. Trans. Roy. Soc.* **1857**, *147*, 145.

(4) (a) For instance, see Professor Reetz's unsurpassed electrochemical synthesis[4b,c] (see elsewhere for a discussion of this interesting method)[2b] as well as the papers cited in refs 15−19 herein. (b) Reetz, M. T.; Helbig, W.; Quaiser, S. A.; Stimming, U.; Breuer, N.; Vogel, R. *Science* **1995**, *267*, 367. (c) Reetz, M. T.; Helbig, W. *J. Am. Chem. Soc.* **1994**, *116*, 7401. (d) Reetz, M. T.; Quaiser, S. A. *Angew. Chem., Int. Ed. Engl.* **1995**, *34*, 2240. (e) Reetz, M. T.; Helbig, W.; Quaiser, S. A. *Chem. Mater.* **1995**, *7*, 2227. (f) Reetz, M. T.; Quaiser, S. A.; Breinbauer, R.; Tesche, B. *Angew. Chem., Int. Ed. Engl.* **1995**, *34*, 2728. (g) Reetz, M. T.; Lohmer, G. *Chem. Commun.* **1996**, 1921. (h) Reetz, M. T.; Breinbauer, R.; Wanninger, K. *Tetrahedron Lett.* **1996**, *37*, 4499. (i) Review: Reetz, M. T.; Helbig, W.; Quaiser, S. A. In *Active Metals*; Fürstner, A., Ed.; VCH Publishers: 1996; New York, Chapter 7, pp 279−297. (j) See also ref 54c cited below.

S0002-7863(97)00510-6 CCC: $14.00

contrary, statements are common in the nanocluster literature reflecting frustration over the empiricism in existing nanocluster synthetic routes.[5]

The state of modern *mechanistic investigations of nanocluster formation* is even more primitive. Specifically, there are no prior kinetic and mechanistic investigations of the formation pathway of a modern, compositionally well-defined nanocluster. Our recent review of the literature of nanoclusters in catalysis reveals three main reasons for this dearth of mechanistic studies:[2] (i) only recently have the first examples of *compositionally fully defined*, prototype nanoclusters appeared, that is, ones suitable for in-depth mechanistic studies;[1,2b] (ii) the available ways to monitor the formation of nanoclusters in real time are limited;[6] and hence (iii) mechanistic chemists have simply not tackled this area previously. The nanocluster literature is, again, replete with calls for modern kinetic and mechanistic studies,[7] work required to obtain the understanding necessary to construct designed nanocluster syntheses.

A Brief Review of the Classical Mechanistic Literature on the Formation of Colloids and Nanoclusters. An appreciation for the existing literature on the mechanism of formation of classical colloids is necessary in order to understand the work herein. A comprehensive list of the 19 prior papers since 1950 providing mechanistic data on colloid or nanocluster formation has been compiled in Table A (Supporting Information) for the interested reader, along with brief summaries covering the contents of each paper. In the following paragraphs, a short summary of the key points of the most useful classical to most recent papers is presented.

Scheme 1. LaMer's Mechanism Consisting of Nucleation Followed by Diffusive, Agglomerative Growth (S = Sulfur)

(a) Nucleation from Supersaturated Solution: $nS \rightleftharpoons S_n$

(b) Diffusion-Controlled Growth: $S_n + S \rightleftharpoons S_{n+1}$

The Classic LaMer Mechanism. In the 1950s, LaMer and co-workers studied extensively the formation of sulfur sols, from which they developed their mechanistic scheme for the formation of colloids or clusters in homogeneous, initially supersaturated solutions.[8,9] Their widely cited mechanism, Scheme 1, assumes that homogeneous nucleation (via a stepwise sequence of bimolecular additions) occurs until a nucleus of critical size is obtained.[10] In accordance with statistical mechanics (the "fluctuation theory" cited by LaMer)[8b] the energy barrier to nucleation can only be surmounted in supersaturated solutions, where the probability of such bimolecular encounters is sufficiently high. Others, however, dispute LaMer's nucleation mechanism, finding kinetics in gold sol formation that are incompatible with the supersaturation hypothesis.[11]

In the LaMer mechanism, further growth on the nucleus is spontaneous but diffusion-limited (i.e., limited by diffusion of

(5) (a) Bradley correctly notes on p 490 of his scholarly review[1f] that "perhaps the most irritant in colloid synthesis is irreproducibility". He goes on to note that we really "don't have any idea on how to control particle size through the proper selection of polymers, solvents, precursors, reducing agents, or metal precursors". He concludes that "the true control of particle size remains the most attractive goal for the synthetic chemist in this field". (b) G. Schmid echoes these points, saying on p 3 elsewhere[1g] that "the genesis of the formation of distinct large, ligand stabilized clusters is so complex that no reactions can be planned using stoichiometric rules. On the contrary, it is left to chance if larger clusters are formed at all". (c) See also the quotes and references provided in footnote 5g elsewhere.[20a]

(6) (a) The detection of nanocluster sizes and size-distributions is most commonly done by TEM (transmission electron microscopy), although reports of changes induced by the TEM beam are fairly frequent;[1] additional lead references of TEM-induced changes of nanoclusters are provided in ref 18 elsewhere.[20a] One might believe that light scattering is the method of choice for size-distribution monitoring, but this is really only 100% true when a single-size, monodispersed nanocluster is present.[6b] (b) Briefly, the reason that light scattering is not the method of choice when a distribution of size-nanoclusters is present is that it involves a nonlinear least-squares fit to a multiexponential (i.e., instead of a single exponential) function. Hence, the resulting solution cannot be guaranteed to be the true global minima for the problem. We thank Dr. Jess Wilcoxon, of Sandia National Labs, for his expert assistance with this point.

(7) (a) Matijevic, E. *Chem. Mater.* **1993**, *5*, 412. Professor Matijevic notes "The ultimate aim in the studies of chemical mechanisms in the precipitations from homogeneous solutions is to develop some general principles, that would make predictable the processes leading to the formation of uniform particles". Another interesting paragraph is "The quantitative explanation of a process by which a huge number of subunits aggregate into *identical* large particles has not been developed as of yet. It is also not clear why in some instances the final particles are spherical and in others they appear in different geometric forms, yet are of the same chemical composition." (b) Beattie, J. K. *Pure Appl. Chem.* **1989**, *61*, 937 calls for "Understanding the kinetics and mechanisms of the complex dynamics of particle formation and growth is necessary before particles of a particular size can be readily prepared". (c) Steigerwald, M. L.; Brus, L. *Acc. Chem. Res.* **1990**, *23*, 183. These authors note on p 184 that despite kinetic precipitations being one of most common routes to size-controlled, monodispersed particles, "... the mechanisms are not well understood". These authors also specifically note the concept of "living polymers" (see p 184) in the case of their CdSe or CdS nanoclusters. (d) Weller, H. *Angew. Chem., Int. Ed. Engl.* **1993**, *32*, 41−53. Weller perhaps says it best in this insightful review when, in talking about the recent advances in synthesis (inverse micelles vessicles, Langmuir-Blodgett films, glasses, polymer films, clay minerals, zeolites, porous TiO_2, etc.), that "these methods are doomed, however, because the individual reaction steps of seed formation (i.e., nucleation), the growth, and stabilization of the small particles are not well enough understood and, hence, cannot be sufficiently controlled".

(8) (a) LaMer, V. K.; Dinegar, R. H. *J. Am. Chem. Soc.* **1950**, *72*, 4847. (b) LaMer, V. K. *Ind. Eng. Chem.* **1952**, *44*, 1270.

(9) Reiss, H. *J. Chem. Phys.* **1951**, *19*, 482.

(10) (a) The nanoparticle nucleus free energy as a function of nucleus size is given by the equation[10b]

$$\Delta G_{(\text{nucleus})} = \Delta G_{(\text{bond formation})} + \Delta G_{(\text{surface tension creation})}$$

where the two terms are intrinsically of opposite sign (i.e., bond formation favors, while surface tension disfavors, nucleus formation). Alternatively, one can express this as[10b]

$$\Delta G_{(\text{nucleus})} = n(\Delta G_{\text{formation, bulk}} - \Delta G_{\text{formation, free atom}}) + \sigma A$$

where n the total number of atoms in the particle, σ is the surface tension, and A the particle surface area.[10b] The key result of the opposing signs of the bond formation and surface free energy terms is a ΔG vs particle size (i.e., vs n) curve that looks qualitatively as follows

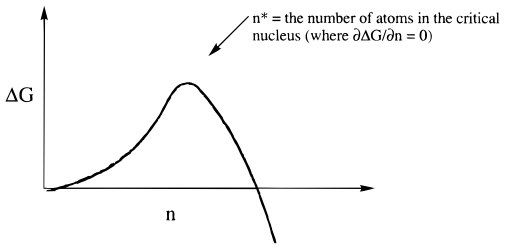

In terms of radii,[8b] $\Delta G = 4\pi\sigma\,(r^2 - [2r^3/3r^*])$ (with the curve maximum ($\partial\Delta G/\partial r = 0$) at r^*), where r is the nucleus radius, r^* is the critical nucleus radius, and σ is again the surface tension. (b) Everett, D. H. *Basic Principles of Colloid Science*; Royal Society of Chemistry: London, 1988; p 56.

(11) (a) Turkevich, J.; Stevenson, P. C.; Hillier, J. *Faraday Discuss. Chem. Soc.* **1951**, *11*, 55. (b) As with nearly all science, if one scours the older literature in sufficient detail, *hints* of what was at first believed to be completely new can be uncovered in earlier work.[11a,14] Turkevich's work, a classic for its time, verbally describes an "organizer" theory of nucleation but fails to provide a detailed mechanism describing the underlying, kinetically dominant elementary steps; hence, that work has been little cited in the intervening 46 years. However, these authors do note, on p 70, that it is hard to understand "the marked temperature dependence of the rate of nucleation" from the point of view of supersaturation-based nucleation. They also see sigmoidal reaction curves when *citrate* is used as the reductant. Note that, with the mechanistic understanding presented herein, Turkevich's 1951 and the present, 1997 work can now be seen to be connected conceptually in that both convert a slow reductant (citrate or H_2 without catalyst, respectively) into a *kinetically facile reductant* (the partially oxidized citrate intermediate, acetone dicarboxylate, or H_2 oxidatively added to a catalyst, respectively). This connection to Turkevich's classic paper is another indicator (see the Discussion) of the significance and broader generality of the mechanistic insights uncovered herein.

the precursor to the nuclei surface).[8a] The LaMer mechanism predicts that as the colloid precursor is consumed, its concentration falls below supersaturation, and hence no more nucleation takes place—thereby achieving the needed *key separation of nucleation and growth in time* that is required for the formation of a near-monodisperse[2] size distribution. Regardless of whether or not the LaMer mechanism is correct in a given case, this separation of nucleation and growth in time is a key for all nonphysically restricted (e.g., nonmicellar)[12] syntheses of near-monodisperse nanoclusters.

The LaMer mechanism has been widely applied in various preparations of near-monodisperse particles in homogeneous solutions,[7a] yet success is often achieved only following tedious, trial-and-error attempts tuning the main variables, such as the concentration of reactants. Generalizations between preparations are few, and the range of possible variations within each preparation is often small; hence, each new colloidal particle requires what is tantamount to a new synthetic strategy. It is also now believed that the LaMer mechanism is, as a mechanistic chemist would expect, rigorously appropriate only to the system it was developed for: sulfur sols, and other, closely analogous systems.[13] This can explain why others have referred to the LaMer mechanism as "overcited" [7a] (perhaps much fairer to LaMer's pioneering work would be the term "inappropriately cited"), a phenomenon which really only points to the dearth of new, broadly applicable and kinetically verified alternative mechanisms in the intervening nearly 50 years. If one adds that any postulated mechanism needs to be clearly expressed in terms of the usual elementary (or pseudoelementary, *vide infra)* chemical equations and not just words and phenomenology, so that others can test, use, and adapt the otherwise only "implied" mechanisms,[11,14] then there has been no truly new mechanistic paradigm governing nanocluster formation reactions since the 1950s.[8−14]

In more recent studies which illustrate the importance of key reaction variables, platinum colloids were obtained in a *variety of shapes* from the same solution but under different conditions and combinations of reducing and protective (surfactant) agents.[14] In a separate study, El-Sayed and co-workers reported the synthesis of shape-controlled platinum particles by varying only the surfactant-to-metal ratio, but conclude their paper with "the mechanism of shape- or morphology-dependent synthesis of colloidal nanoparticles is not yet known".[15] The latter ratio has been used previously in the synthesis of size-controlled gold colloids, in which the authors first *assume* their reaction is thermodynamically controlled, and then derive a thermodynamic expression (based on surface energies) to account for surfactant-mediated particle stabilization.[16] Alternatively, other authors report the use of surfactant as a means to gain *kinetic control*[17] over the particle growth.[18] These studies again illustrate the *lack of fundamental understanding* of how the kinetic, thermodynamic,[16,19] or other factors influence the underlying mechanisms in these and other interesting systems (Table A, Supporting Information).

$P_2W_{15}Nb_3O_{62}^{9-}$ Polyoxoanion- and Bu_4N^+-Stabilized $Ir(0)_{\sim 300}$ Nanoclusters

Recently, we reported the discovery of novel $P_2W_{15}Nb_3O_{62}^{9-}$ polyoxoanion- and Bu_4N^+-stabilized $Ir_{\sim 190-450}$ and $Ir_{\sim 640-1460}$ nanoclusters, hereafter referred to as $Ir(0)_{\sim 300}$ and $Ir(0)_{\sim 900}$ nanoclusters, respectively.[20] A pictorial representation of these unusual—and compositionally well characterized—nanoclusters is presented in Figure 1.

The overall stoichiometry established previously[20a] for the formation of the $Ir(0)_{\sim 300}$ nanoclusters is shown in Scheme 2. A comparison presented elsewhere[2] (i.e., to the small number of other compositionally well-characterized transition metal nanoclusters in the literature) reveals that these $Ir(0)_{\sim 300}$ and $Ir(0)_{\sim 900}$ nanoclusters are without precedent in their "*combination* of isolability, known molecular formula as well as their retention of catalytic activity",[2] plus their novel polyoxoanion component.

(12) Alivisatos, A. P.; Harris, A. L.; Levinos, M. L.; Steigerwald, M. L.; Brus, L. E. *J. Chem. Phys.* **1988**, *89*, 4001.

(13) (a) The first specific problem in generalizing the LaMer mechanism to other systems is that, as the literature indicates, homogeneous nucleation does not always follow LaMer's supersaturation theory; Turkevich calls it a "theory of great tradition" but ultimately rejects it for his "organizer" mechanism, in which he envisioned a more gradual nucleation process.[11] However, in cases such as Turkevich's, and if LaMer's supersaturation theory is rejected, the separation in time between nucleation and growth required to make near-monodisperse particles is unexplained (i.e., it can no longer be explained simply by staying above or below supersaturation). Another problem in generalizing the LaMer mechanism to other systems is that, at the end of the nucleation period, nuclei aggregation ($A_n + A_m \rightarrow A_{n+m}$)[13b] or Ostwald ripening to generate more stable nuclei ($A_n + A_m \rightarrow A_{n-1} + A_{m+1}$) may have already occurred[7a] resulting in a range of nuclei sizes. Adding to the problems in synthesizing near-monodispersed particle distributions under the LaMer mechanism and its variants is the fact that diffusion is not always the rate-determining step in particle growth; instead, incorporation of the new atom onto the particle surface can be rate-determining, which in turn will depend on the particle's surface area or volume.[13c] Lastly, other means for particle growth besides diffusion can occur. In LaMer sols, the particle size distribution, after sharpening with time as expected for diffusive growth,[9] then broadens again, suggesting that there is agglomerative growth,[13d] a topic that has been studied in some detail.[13e] Agglomeration can account for a log-normal shape of the size-distribution function (in which there are more larger than smaller particles)[13f] and for a decay of the catalytic rate in metal colloids.[13g] However, other authors believe that agglomerative phenomena (e.g., Ostwald ripening) are a key to particle uniformity since such steps allow for interparticle size rearrangements.[13h] (b) Fojtik, A.; Weller, H.; Koch, U.; Henglein, A. *Ber. Bunsenges. Phys. Chem.* **1984**, *88*, 969. (c) Overbeek, J. Th. G. *Adv. Colloid Interf. Sci.* **1982**, *15*, 251. (d) Kerker, M.; Daby, E.; Cohen, G. L.; Krahtovil, J. P.; Matijevic, E. *J. Phys. Chem.* **1963**, *67*, 2105. (e) Lin, M. Y.; Lindsay, H. M.; Weitz, D. A.; Ball, R. C.; Klein, R.; Meakin, P. *Nature* **1989**, *339*, 360. (f) Granqvist, C. G.; Buhrman, R. A. *J. Catal.* **1976**, *42*, 477. (g) Melrose, J. R. *J. Chem. Phys.* **1990**, *92*, 4595. (h) Look, J. L.; Bogush, G. H.; Zukoski, C. F. *Faraday Discuss. Chem. Soc.* **1990**, *90*, 345.

(14) Van Rheenen, P. R.; Mc Kelvy, M. J.; Glaunsinger, W. S. *J. Solid State Chem.* **1987**, *67*, 151. Buried in Van Rheenen and co-worker's paper on p 164 is the author's brief mention that the reaction of $H_2PtCl_6^{2-}$ plus $Me_2NH{\cdot}BH_3$ changes color "suddenly after a definite induction period" which they follow by the unproved assertion that this reaction "must certainly be autocatalytic". They go on to mention the ideas of a critical concentration of nuclei and then the "reduction of the remaining $H_2PtCl_6^{2-}$ on these caytalytic sites". However, the lack of kinetic evidence to support or refute these mechanistic assertions and hence the lack of elementary mechanistic steps to summarize exactly the verbally implied mechanism are probable reasons their implied mechanism has gone virtually unnoticed until resurrected by the kinetic evidence and pseudoelementary mechanistic steps presented herein.

(15) (a) Ahmadi, T. S.; Wang, Z. L.; Henglein, A.; El-Sayed, M. A. *Chem. Mater.* **1996**, *8*, 1161. (b) Ahmadi, T. S.; Wang, Z. L.; Green, T. C.; Henglein, A.; El-Sayed, M. A. *Science* **1996**, *272*, 1924.

(16) (a) Whetten, R. L.; Gelbart, W. M. *J. Phys. Chem.* **1994**, *98*, 3544. (b) Leff, D. V.; Ohara, P. C.; Heath, J. R.; Gelbart, W. M. *J. Phys. Chem.* **1995**, *99*, 7036.

(17) (a) Murray, C. B.; Norris, D. J.; Bawendi, M. G. *J. Am. Chem. Soc.* **1993**, *115*, 8706. (b) See, also: Reiss' work.[9]

(18) References covering particle growth,[16,18a,b,19a] and the statistics of types of surface sites[18c] in growing particles: (a) Duff, D. G.; Curtis, A. C.; Edwards, P. P.; Jefferson, D. A.; Johnson, B. F. G.; Logan, D. E. *Chem. Commun.* **1987**, 1264. (b) Friedel, J. *J. Phys. Chem.* **1977**, *38*, Coll. C2, Supplement 7, C2-1. (c) Van Hardeveld, R.; Hartog, F. *Surf. Sci.* **1969**, *15*, 189−230.

(19) (a) Wales, D. J.; Kirkland, A. I.; Jefferson, D. A. *J. Chem. Phys.* **1989**, *91*, 603. (b) Bigot, B.; Minot, C. *J. Am. Chem. Soc.* **1984**, *106*, 6601.

(20) (a) Lin, Y.; Finke, R. G. *J. Am. Chem. Soc.* **1994**, *116*, 8335. (b) Lin, Y.; Finke, R. G. *Inorg. Chem.* **1994**, *33*, 4891. (c) The *average* composition of the $Ir(0)_{\sim 300}$ and $Ir(0)_{\sim 900}$ nanoclusters were demonstrated to be $[Ir(0)_{\sim 300}(P_4W_{30}Nb_6O_{123}^{16-})_{\sim 33}](Bu_4N)_{\sim 300}Na_{\sim 228}$ and $[Ir(0)_{\sim 900}(P_4W_{30}Nb_6O_{123}^{16-})_{\sim 60}](Bu_4N)_{\sim 660}Na_{\sim 300}$, respectively. Note that the $P_2W_{15}Nb_3O_{62}^{9-}$ has formed its anhydride, in the presence of the 1 equiv of H^+ produced in the nanocluster formation reaction, via the reaction $2P_2W_{15}Nb_3O_{62}^{9-} + 2H^+ \rightarrow H_2O + [(P_2W_{15}Nb_3O_{61})_2{-}O]^{16-}$ (see elsewhere for additional discussion of this point).[20a,b]

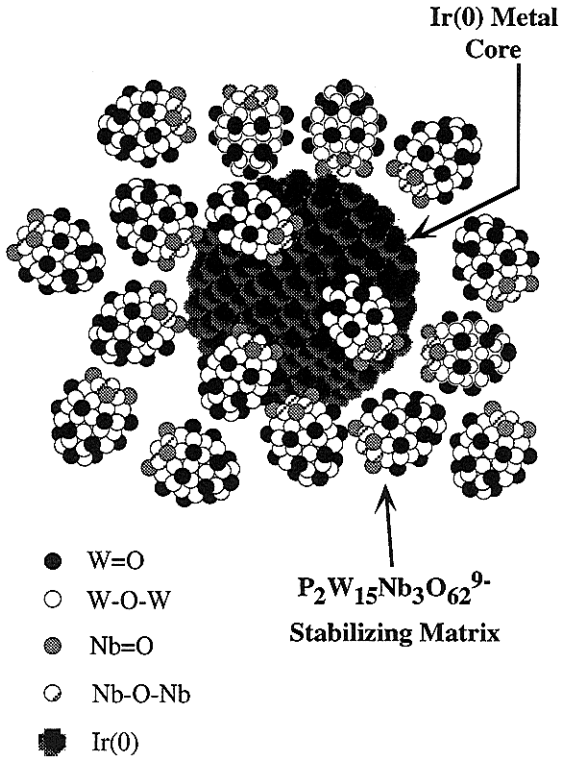

Figure 1. Idealized, roughly-to-scale representation of a $P_2W_{15}Nb_3O_{62}^{9-}$ polyoxoanion and Bu_4N^+ stabilized $Ir(0)_{\sim 300}$ nanocluster, $[Ir(0)_{\sim 300}(P_4W_{30}Nb_6O_{123}^{16-})_{\sim 33}](Bu_4N)_{\sim 300}Na_{\sim 228}$. The Ir(0) atoms are known (by electron diffraction) to be cubic-close packed as shown.[20] For the sake of clarity, only 17 polyoxoanions are shown, the polyoxoanion is shown in its monomeric, $P_2W_{15}Nb_3O_{62}^{9-}$ form (and not as its Nb−O−Nb bridged, anhydride, $P_4W_{30}Nb_6O_{123}^{16-}$ form), and the ∼300 Bu_4N^+ and ∼228 Na^+ cations have been deliberately omitted.

Scheme 2. Average Stoichiometry of Formation of the Polyoxoanion-Stabilized $Ir(0)_{\sim 300}$ Nanoclusters

$$300\ [(1,5\text{-COD})Ir{\bullet}P_2W_{15}Nb_3O_{62}]^{8-} + 750\ H_2 \rightarrow 300\ \bigcirc + 1\ Ir(0)_{\sim 300} + 300\ [P_2W_{15}Nb_3O_{62}]^{9-} + 150\ H^+$$

Furthermore, their high catalytic hydrogenation activity (see Table 1 elsewhere)[2] provides an indirect way—but as shown herein, a very useful and presently one of the most powerful ways—to follow the formation of these Ir(0) nanoclusters. Specifically, their formation is easily detected via their catalytic cyclohexene plus H_2 olefin hydrogenation reaction, eq 1, and its H_2 consumption as precisely monitored by a computer-interfaced, ±0.01 psig pressure transducer.

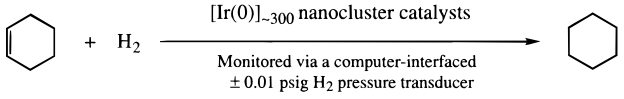

(1)

Also noteworthy is that, without trying and in our first two nanocluster syntheses reactions, we had prepared two nanoclusters ($Ir(0)_{\sim 300}$ and $Ir(0)_{\sim 900}$) close to two of the "magic" (i.e., greater stability)[2] numbers: M_{13}, M_{55}, M_{147}, $\mathbf{M_{309}}$, M_{561}, $\mathbf{M_{923}}$, M_{1415}, and so on.[21] Hence, a kinetic and mechanistic study of the $Ir(0)_{\sim 300}$ and $Ir(0)_{\sim 900}$ nanocluster systems promised to provide mechanistic insights into *why* magic number nanoclusters tend to form.

Herein we present the full details of our kinetic and mechanistic studies of the formation of the $Ir(0)_{\sim 300}$ nanocluster system. Our results provide a completely different mechanism in comparison to the classic LaMer mechanism of (i) nucleation in supersaturated solution and (ii) diffusive growth. Specifically, our results demonstrate that (i) nucleation is achieved via a *low-level, continuous*, slow process in a solution that is far from supersaturated and (ii) a subsequent *autocatalytic surface-growth* step achieves the key separation in time required for a synthesis of near-monodisperse[2] nanoclusters. Moreover, and in contrast to the LaMer mechanism, this autocatalytic surface growth step is normally not diffusion limited.[22,23]

Additional papers have been submitted (i) describing how the above results allow the first successful synthesis of a series of magic number nanocluster distributions centering about four sequential magic numbers, $Ir(0)_{\sim 147}$, $Ir(0)_{\sim 309}$, $Ir(0)_{\sim 561}$ and $Ir(0)_{\sim 923}$,[24] (ii) describing how second row and thus especially active hydrogenation catalysts such as Rh follow a H_2-mass-transfer limitated[23] pathway, one which results in dramatic effects on the nanocluster size distribution, (iii) and revealing how the other main feature of the present mechansim, the autocatalytic surface growth step, is maintained even when mechanisms of initial hydrogen activation besides *cis*-oxidative addition are involved. Only a brief description of the new kinetic method developed herein has been previously communicated.[25]

Experimental Section

(A) Materials. Acetone was purchased from Burdick & Jackson (water content <0.2%) and stored in a Vacuum Atmospheres drybox. Cyclohexene (Aldrich, 99%) was purified by distillation from Na under Ar and stored in the drybox. Acetic acid (99.9%) was dried by distillation with CrO_3 and acetic anhydride and[26] then also stored in the drybox. Water was purged with an Ar stream for 30 min prior to use. Ar and N_2 were prepurified by running these gases over activated (black) BASF O_2-removing Cu catalyst and activated molecular sieves. The precatalyst complex $[Bu_4N]_5Na_3[(1,5\text{-COD})Ir(P_2W_{15}Nb_3O_{62})]$ (**1**)[27a] and the polyoxoanion $[Bu_4N]_9[P_2W_{15}Nb_3O_{62}]$ (**2**)[28] were prepared according to literature procedures. Note that use of our improved preparation and $Bu_4N^+OH^-$ titration procedure[28] (and with careful

(21) (a) The term "magic number" is misleading and thus somewhat controversial. A better term for these clusters is "full-shell" clusters, that is, clusters which possess some extra stability due to their close-packed, full-shell nature, a situation in which each Ir atom therefore has the maximum number of nearest neighbors and thus maximum number of stabilizing, metal−metal bonds. (b) A good discussion of the first "magic number clusters", M_n, but of a different type and for alkali metals (M = Na, K, Cs; n = 2, 8, 20, 40, 58, 92, 138, and so on), plus a good discussion of the difference of these magic numbers from those based on icosahedral or cubo-octahedral structures, is available in Howie, A. *Faraday Discuss.* **1991**, *92*, 1−11.

(22) Instead, the rate-determining step is metal incorporation onto the particle surface, whose rate therefore depends on the particle surface area (i.e., the number of catalytic sites). The resultant particle growth rate should then be a constant.[13c] Such a phenomenon has been reported by Turkevich and co-workers,[11a] another observation connecting that classic and the present work.[11b]

(23) We have, however, uncovered a case (Rh(0) nanocluster formation) where diffusion-limited kinetics are seen, including its dramatic effect on the nanocluster size distribution: Aiken, J. D., III; Finke, R. G. *J. Am. Chem. Soc.* In press.

(24) Watzky, M. A.; Finke, R. G. *Chem. Mater.* **1997** In press.

(25) Watzky, M. A.; Finke, R. G. Submitted for publication.

(26) Orton, K. J. P.; Bradfield, A. E. *J. Chem. Soc.* **1927**, 983.

(27) (a) Pohl, M.; Lyon, D. K.; Mizumo, N.; Nomiya, K.; Finke R. G. *Inorg. Chem.* **1995**, *34*, 1413. (b) The $(1,5\text{-COD})Ir(solvent)_2^+$ complex[27c] seen as part of the mechanism deduced herein (see Scheme 3) is a well-precedented, meta-stable complex, one which is in fact used in the synthesis of the precursor complex, **1**. (c) Sievert, A. C.; Mutterties, E. L. *Inorg. Chem.* **1981**, *20*, 489.

(28) (a) Weiner, H. W.; Aiken, J. D., III; Finke, R. G. *Inorg. Chem.* **1996**, *35*, 7905. (b) It is important that the titration of the $4H^+$ in $H_4P_2W_{15}Nb_3O_{62}^{5-}$ using $Bu_4N^+OH^-$ be performed exactly as described,[28a] since even a single drop of excess OH^- causes variable induction periods and hydrogenation rates (typically shorter and faster, respectively).

attention to the details therein to avoid adding even 1 drop too little or too much $Bu_4N^+OH^-$) is required for the synthesis of the best, highest purity $[Bu_4N]_9[P_2W_{15}Nb_3O_{62}]$.

(B) Hydrogenations. (1) Apparatus. The nanocluster formation and hydrogenation reactions were carried out as previously described in detail,[20b] in a Fischer-Porter bottle modified with Swagelock TFE-sealed Quick-Connects and connected to a H_2 line and a Omega PX-621 pressure transducer interfaced through an Omega WB-35 A/D converter to an IBM PC-XT, using the RS-232 module of Lotus Measure (see Figure 6 elsewhere for a drawing and further details of this hydrogenation apparatus).[20b] The progress of an individual hydrogenation reaction was monitored by the loss of H_2 pressure (over periods ranging from 1−36 h), and the data was then fed into, and worked up via, Lotus 1-2-3. Five types of control experiments were done previously to ensure that the apparatus provided both a precise and accurate picture of the H_2 uptake reaction[20b] (i.e., controls showing: that it did not admit detectable atmospheric O_2 ($\ll$1 mM); that it reproduced faithfully the literature rate for a known hydrogenation catalyst; that the apparatus did not leak appreciable H_2 pressure; plus other types of controls[20b]).

(2) Nanocluster Formation and Cyclohexene Hydrogenation with 1 as Precatalyst: Standard Conditions. A typical experiment followed closely our established protocol.[20b] In the drybox, 20.5 ± 1.0 mg (3.61 ± 0.18 μmol) of the precatalyst complex $[Bu_4N]_5Na_3[(1,5\text{-COD})Ir{\cdot}P_2W_{15}Nb_3O_{62}]$ (**1**) were dissolved in 2.5 mL of acetone, followed by the addition of 0.50 ± 0.03 mL (4.94 ± 0.30 mmol) of cyclohexene. The clear, bright-yellow solution (containing 1.20 ± 0.06 mM of **1** and 1.65 ± 0.10 M of cyclohexene) was then transferred to a clean, 22 × 175 mm disposable Pyrex culture tube containing a 5/8″ x 5/16″ magnetic stir bar. The tube was placed in a Fischer-Porter bottle modified with Swagelock TFE-sealed Quick-Connects (as described above); the bottle was then sealed, brought out of the drybox, and placed into a Fischer Scientific 9100 temperature-controlled (±0.1 °C) bath at 22.0 ± 0.1 °C unless otherwise indicated. In the mean time, the H_2 line and pressure transducer had been evacuated for at least 1 h under vacuum (≤100 mmHg) and then refilled with prepurified H_2, with the goal of removing trace oxygen and water from the apparatus and its lines. Next, the Fischer-Porter bottle was connected between the now O_2 and H_2O free pressure transducer and the H_2 line using the Quick-Connects. The Fischer-Porter bottle was then purged 15 times with approximately 40 psig H_2 (15 s per purge), the H_2 pressure was set to a desired value (typically 40 ± 0.5 psig) in less than 10 s, and the connection between the Fischer-Porter bottle and the H_2 line was closed (see Figure 6 provided elsewhere as needed).[20b] The Fischer-Porter bottle was shaken vigorously for 15 s (to equilibrate the gas and solution phases, thereby also initiating fully the hydrogenation reaction), and then vortex was stirred at 570 ± 30 rpm. The H_2 pressure vs time data collection was then started, with this time designated as $t = 0$.

(C) Controls for the Pseudoelementary Model:[29] Cyclohexene Hydrogenation with 1 as Precatalyst. These control experiments were needed to test the applicability of using a pseudoelementary step[29a−c] to treat the kinetic data, a concept that will be explained and developed in the Results and Discussion sections. For now, these experiments can be viewed empirically—do changes in the olefin and H_2 reactant concentrations affect the observed H_2 pressure vs time curves?

(1) Effect of Initial Cyclohexene Concentration. In a series of nine individual experiments that were otherwise analogous to the Standard Conditions cited above, in the drybox 20.5 ± 1.0 mg (3.61 ± 0.18 μmol) of **1** were dissolved in, respectively, 2.25−2.75 mL of acetone (giving the usual clear, bright-yellow solution), followed by the addition of 0.75−0.25 mL of cyclohexene (3 mL total; 0.8−2.5 M), in 0.05−0.15 mL increments, to yield the nine separate experiments. This solution was placed in a 22 × 175 mm disposable Pyrex culture tube containing a 5/8″ × 5/16″ magnetic stir bar. The culture tube for an individual experiment (i.e., with one of the nine prechosen amounts of cyclohexene) was then placed in the usual Quick-Connect-equipped Fischer-Porter bottle and brought out of the drybox, and the reaction was started via the usual sequence of H_2 purges and then shaking (see the Standard Conditions cited above). The results are shown in Figure 6.

(2) Effect of Initial Hydrogen Pressure. Nine separate standard solutions of **1** in acetone were prepared exactly as detailed in the Standard Conditions section. The constant temperature bath was set at 22.0 ± 0.1 °C, and the nanocluster formation and hydrogenation reaction was initiated with the usual series of H_2 flushes and then shaking, all exactly as detailed in the Standard Conditions section. The only difference in these nine separate, but otherwise identical, experiments is that the H_2 pressure was varied from 3.5 to 48.5 psig, in 3−7 psig increments. The results are shown in Figure 7.

(D) Curvefits of The Hydrogen Uptake Data. (1) Curvefitting Program. Curvefitting of the H_2 pressure (or, equivalently, the cyclohexene) vs time data was performed using a nonlinear regression subroutine (RLIN), available in the IMSL Statistical Library, which uses a modified Levenberg-Macquard algorithm.[30] Calculations were done on an IBM/AIX workstation. A FORTRAN program was written that reads the list of input data points, defines the analytical expression to which the data points will be curvefitted, asks for initial guesses of the variables (k_1 and k_2), and calls the appropriate RLIN subroutine. (The short programs for importing, exporting, and formatting the data to fit a FORTRAN format as well as the main curvefitting program are detailed in the Supporting Information.) Calculated values of the variables are obtained as output, along with details on the regression. A range of initial guesses of the variables (i.e., the widest possible range of empirical initial guesses which still allowed the subroutine to converge) was employed in order to avoid local minima.

As a control, the program was tested and verified before use via a calculated, "mock" data set obtained by computing a set of input concentration vs time data for arbitrary k_1 and k_2 values (5.000×10^{-3} and 1.000, respectively) and then testing the program on the mock data set. The program and resultant curvefit faithfully found the k_1 and k_2 values ($\pm 0.001 \times 10^{-3}$ and ±0.001, respectively) for the mock data set. Indeed, during the course of our studies the modified Levenberg-Macquard algorithm was found to be quite robust for our system, presumably due to the fact that the program switches as needed between two search algorithms, depending upon whether it is far from or close to the minimum.[30]

(2) Data Handling. The pressure transducer follows the H_2 pressure above the solution, while the hydrogen uptake via the cyclohexene hydrogenation reaction is, of course, in solution. The needed relation between these two was obtained by treating the hydrogen atmosphere above the solution as an "hydrogen reservoir" (originally developed and employed first elsewhere)[31] as follows: one sets $\Delta n(H_2)_{solution} = \Delta n(H_2)_{gas}$ where $\Delta n(H_2)_{gas} = \Delta P(H_2)_* V_{gas}/RT$, so that $\Delta[H_2] = (\Delta P(H_2)_* V_{gas})/(RT_* V_{solution})$. Also, sometimes it is desirable to express the H_2 loss in terms of its equivalent cyclohexene loss; this was done via their established, 1:1 stoichiometry (i.e., Δn(cyclohexene) = $\Delta n(H_2)_{solution}$).[20b] For our apparatus, V_{gas} = 97 mL and $V_{solution}$ = 3 mL, so that at T = 22 °C we have $\Delta[\text{cyclohexene}]_M = 0.0909_* \Delta P(H_2)_{psi}$.

Only the data points prior to the consumption of half of the initial H_2 or cyclohexene concentration were used in the curvefitting process, in order to assure the validity of the pseudoelementary model, *vide infra* [i.e., late in the reaction the cyclohexene concentration approaches zero, and hence the kinetics of the cyclohexene hydrogenation reaction (the third step, eq 2c, *vide infra*) are no longer sufficiently fast, so that the cyclohexene hydrogenation reaction now also affects the observed kinetics, rather than serving as a pseudoelementary, "reporter" reaction, *vide infra*].

The consumption of cyclohexene as a function of time was curvefit to eq 4 (*vide infra*), yielding values of k_1 and k_2 (the value of k_2 is a function of, and thus had to be corrected for, the initial concentration of precatalyst 1; see the discussion available in a footnote[32] and in the Appendix). Error bars are typically ±10% unless specified otherwise

(29) For an introduction to the concept of pseudoelementary reactions, a concept created for and often necessary with the kinetics of more complex systems, see the pioneering work of Professor Richard Noyes: (a) Noyes, R. M.; Field, R. J. *Acc. Chem. Res.* **1977**, *10*, 214. (b) Noyes, R. M.; Field, R. J. *Acc. Chem. Res.* **1977**, *10*, 273. (c) Field, R. J.; Noyes, R. M. *Nature* **1972**, *237*, 390.

(30) Press, W. H.; Flannery, B. P.; Teukolsky, S. A.; Vetterling, W. T. *Numerical Recipes*; Cambridge University: Cambridge, 1989.

(31) Lyon, D. K. Ph.D. Dissertation, University of Oregon, 1990; see pp 142−145.

(and are not specifically shown in the figures to avoid cluttering them).

(E) Cyclohexene Hydrogenation with 1 as Precatalyst: Quantitative Studies. (1) Effect of Added Polyoxoanion. In a series of seven independent experiments differing in only the amount of added $[Bu_4N]_9[P_2W_{15}Nb_3O_{62}]$, **2**, in the drybox, 20.5 ± 1.0 mg (3.61 ± 0.18 μmol) of **1** were dissolved in 2.5 mL of acetone to give the usual clear, bright-yellow solution. A predetermined amount of **2** was added (ranging from 9.5 to 37.6 mg or 0.4−1.7 equiv vs **1**, in increments of 3−7 mg, seven experiments total), followed by the addition of 0.50 ± 0.03 mL (1.65 ± 0.10 M) of cyclohexene. (The mixtures containing 0.6 or more equiv of **2** turned cloudy, presumably due to the low solubility of the polyoxoanion, **2**, in presence of cyclohexene.) Each solution was then transferred in the usual way to a separate culture tube, which was in turn placed in a Quick-Connects-equipped Fischer-Porter bottle; this reaction vessel was then brought out of the drybox and thermostatted at 22.0 ± 0.1 °C, and the nanocluster formation and olefin hydrogenation reaction was started exactly as in the Standard Conditions section. The results are shown in Figure 10.

(2) Effect of Added Water. In a series of seven independent experiments differing in only the amount of added H_2O, in the drybox, 20.5 ± 1.0 mg (3.61 ± 0.18 μmol) of **1** were dissolved in 2.5 mL of acetone to give the usual clear, bright-yellow solution. A predetermined amount of H_2O was added (ranging from 25 to 225 μL or 480−3640 total equiv vs **1**, in increments of 25−50 μL; seven experiments total), followed by the addition of 0.50 ± 0.03 mL (1.65 ± 0.10 M) of cyclohexene. (The mixtures containing 1270 or more total equiv of H_2O turned cloudy, presumably due to a decreased solubility of **1** and the other reactants in the presence of H_2O.) Each solution was then transferred in the usual way to a separate culture tube, which was placed in a Quick-Connects-equipped Fischer-Porter bottle, which in turn was brought out of the drybox, thermostatted at 22.0 ± 0.1 °C, and the nanocluster formation and olefin hydrogenation reaction was started exactly as in the Standard Conditions section. Black, completely insoluble $Ir(0)_{bulk}$ eventually precipitates from these runs (especially with higher amounts of H_2O; see the Results section). The results are shown in Figure 11.

(3) Effect of Added Acetic Acid. In a series of four independent experiments differing in only the amount of added HOAc, in the drybox, 20.5 ± 1.0 mg (3.61 ± 0.18 μmol) of **1** were dissolved in 2.5 mL of acetone to give the usual clear, bright-yellow solution. A predetermined amount of HOAc was added (ranging from 1 to 5 μL or 4.7−23.5 equiv vs **1**, in 1−2 μL increments; four experiments total), followed by the addition of 0.50 ± 0.03 mL (1.65 ± 0.10 M) of cyclohexene. All four mixtures remained clear. Each solution was then transferred in the usual way to a separate culture tube, which was placed in a Quick-Connects-equipped Fischer-Porter bottle; this reaction vessel was brought out of the drybox and thermostatted at 22.0 ± 0.1 °C, and the nanocluster formation and olefin hydrogenation reaction was started exactly as in the Standard Conditions section. When these particular solutions were kept for several days or weeks, completely insoluble, black $Ir(0)_{bulk}$ deposits. The results are shown in Figure S4 of the Supporting Information.

(4) Effect of Temperature. In a series of six independent experiments differing only in their reaction temperature, six separate solutions of **1** in acetone were prepared exactly as detailed in the Standard Conditions section. A solution was brought out of the box (i.e., one solution for one experiment at a time), thermostatted at one of the prechosen six temperatures ranging from 10.0 to 47.0 ± 0.1 °C (in increments of 5−10 °C), the H_2 pressure was set at 40.0 ± 0.5 psig, and the nanocluster formation and olefin hydrogenation reaction was started exactly as in the Standard Conditions section. The results are shown in Figure S5 of the Supporting Information.

(32) As shown in more detail in the Appendix, in the pseudoelementary model (*vide infra*) (a) we obtain kinetic information on the net reaction 2d by following −d[cyclohexene]/dt. (b) The net reaction 2d in fact has the kinetics of steps 2a,b, that is $-d[A]/dt = k_1[A] + k_2[A]([A]_0 - [A])$ (see eq 3). (c) We, therefore, curve-fit the loss of cyclohexene to $-d[\text{cyclohexene}]/dt = k_{1(\text{fit})}[\text{cyclohexene}] + k_{2(\text{fit})}[\text{cyclohexene}]([\text{cyclohexene}]_0 - [\text{cyclohexene}])$. (d) In addition, since the stoichiometry is (see eq 2d) $d[\text{cyclohexene}]/dt \sim 1400\, d[A]/dt$ and $[\text{cyclohexene}] \sim 1400[A]_0$, we find that $k_1 = k_{1(\text{fit})}$ while $k_2 \sim 1400k_{2(\text{fit})}$ (where ∼1400 is the exact ratio of $[\text{cyclohexene}]_0/[1]_0$).

(F) Key Control Demonstrating that the More Direct Monitoring of the Nanocluster $Ir(0)_n$ Formation via the Evolution of Cyclooctane Gives Identical Rate Constants, k_1 and k_2, within Experimental Error. (1) Gas−Liquid Chromatography. GLC was performed on a Hewlett Packard HP-5890 GLC equipped with a HP-3395 integrator, a Alltech DB-1 capillary column (30 m × 0.25 mm), and a flame ionization detector. The injector was maintained at 180 °C, the detector at 200 °C. The following column temperature program was used in all GLC studies: initial temperature of 35 °C for 4.0 min, ramped at 15 °C/min to a final temperature of 200 °C and held there for 1.0 min, followed by cooling back to 35 °C. Under the experimental conditions, a retention time of 2.5 min was found for acetone, of 6.5 min for toluene, and of 9.7 min for cyclooctane.

(2) Determination of the Evolved Cyclooctane vs Time Curve during Nanocluster Formation and Cyclohexene Hydrogenation with 1 as Precatayst and under Standard Conditions. Using a bright-yellow solution of 1.2 ± 0.06 mM of **1** and 1.65 ± 0.1 M of cyclohexene in acetone (containing 1 μL of toluene as a GLC internal standard), a Standard Conditions cyclohexene hydrogenation was started with an initial pressure of 40.0 psig. Eight total reaction runs were performed; each run was stopped by releasing the H_2 pressure at a specific time (t = 1.75, 2.5, 3.25, 4.1, 5.0, 6.1, 7.0, and 24 h), and an aliquot was taken for GLC analysis as described in the "GLC Sampling" section below. The amount of cyclooctane evolved vs time was determined from the relative peak area of cyclooctane vs the toluene internal standard. Also, an absolute calibration curve of GLC peak area vs concentration of cyclooctane was obtained and then used to determine independently the amount of cyclooctane evolved. The results from both methods agreed within 15%.

(3) GLC Sampling. The Fischer-Porter bottle was sealed, removed from the H_2 line, and placed in the drybox antechamber, in which it was kept for ca. 10 min before being brought into the drybox. (Despite the necessary lack of a temperature bath and magnetic stirrer in the antechamber, i.e., for the 10 min, the resultant induction period and rates are not affected within experimental error compared to a "Standard Conditions" run performed as normal and without this sampling step.) In the drybox the H_2 pressure was released and the reaction time (t) recorded. An aliquot was taken from the solution and placed in a screw-capped vial for later GLC analysis. The Fischer-Porter bottle was sealed, taken out of the drybox, and placed back on the H_2 line. The cyclohexene hydrogenation was started with an initial pressure of 40.0 psig as described in the Standard Conditions section above, and the initial time, t_i, was recorded. The results are shown in Figure 8.

(4) Curvefits of the Cyclooctane Evolution Data. The data points were curve-fit exactly as described above for the hydrogenation data (see section D(1)) and using the same analytic function for the nucleation and autocatalysis psuedoelementary step mechanism, eq 4, *vide infra*. The resultant curvefit is shown in Figure 8, and the computed and k_1 and k_2 values are given in the text.

(G) Transmission Electron Microscopy (TEM). (1) Sample Preparation. The solutions used for these TEM experiments were just those prepared and first run exactly as described above in the Standard Conditions and Quantitative Studies sections. However, at the end of a given run (i.e., at a minimum of 1.5 times the time needed to fully reduce the amount of cyclohexene present, see Figure 7 elsewhere),[20b] the Fischer-Porter bottle was detached from the hydrogenation line via its Quick-Connects, brought back into the drybox, and its acetone solution was quantitatively transferred with a pipette into a clean, 5 mL centrifuge tube. The tube was then clamped to a ring-stand, and the usual dark-brown suspension of Bu_4N^+ and $P_2W_{15}Nb_3O_{62}^{9-}$ polyoxoanion-stabilized nanoclusters was allowed to separate over 1−2 h. In the runs with excess polyoxoanion (i.e., section E(1)), no suspension was present. A small amount (usually < 0.5 mL) of anhydrous, degassed diethyl ether was then added slowly (dropwise over 5 min, without stirring) until the solution became opaque, but the addition of ether was halted before a precipitate was observed. After *ca.* 2 h of settling, the light brown supernatant was carefully removed with a pipette, and the precipitate was allowed to dry overnight in the drybox.

In one batch of samples, no solvent was added, and the dry nanocluster samples in screw-capped vials were sent as solids to the

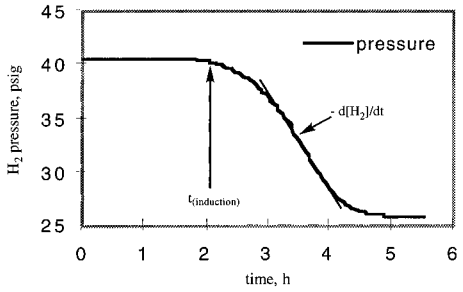

Figure 2. Hydrogen uptake curve under standard conditions, plus two useful definitions: the induction time, $t_{induction}$, and the rate of hydrogen loss, $-d[H_2]/dt$.

University of Oregon for TEM. There, 1 mL of acetonitrile was added, in air, just before a TEM was obtained, Figure 12.

In what was actually an earlier TEM sample preparation method which proved to be less optimum (see the Results section), 1 mL of acetonitrile solvent was added in the drybox, and the residue was dissolved with gentle shaking. The resulting dark-brown solution was placed in a screw-cap vial and kept in the drybox for 6 weeks before being sent to the University of Oregon for the TEM analysis shown in Figure 13.

(2) Sample TEM Analyses. TEM analyses were performed as before[20] at the University of Oregon with the expert assistance of Dr. Eric Schabtach, using the sample preparation procedure and using a Philips CM-12 TEM with a 70 μm lens operating at 100 kV and with a 2.0 Å point-to-point resolution, as described in detail previously.[20a] Typically, TEM pictures of each sample were taken at three different magnifications (100, 200, and 430 K) in order to obtain information about the sample in general (100 K), plus a closer visualization of the clusters (430 K). A number of control experiments were done previously which provided good evidence that results are truly representative of the sample and that the sample is not perturbed by application of the TEM beam[20a] [e.g., controls showing that varying the sample spraying method (in air or under N_2) or depositing the sample as a drop and letting it dry did not change the results; controls showing that changing the beam voltage from 40 to 100 kV, or changing the exposure time (seconds vs minutes), did not change the images; other controls have been done as well].[20a]

Results

Standard H_2-Uptake Curve and Useful Definitions. As represented in Figure 2, the nanocluster formation reaction and its accompanying cyclohexene hydrogenation reaction have an induction period of 2.0−2.5 h, defined as the time until the H_2-loss rate is ≥0.05 psig/2.5 min (the previously employed definition based on the minimum, reproducibly detectable pressure change).[33] The Standard Conditions detailed in the Experimental Section (1.20 mM [**1**], 1.65 M [cyclohexene], 22 °C and 40 psig H_2) were employed throughout unless noted otherwise. A second useful definition and measurement is the slope, $-d[H_2]/dt$, of the linear part in the middle section of the hydrogen uptake curve, $-d[H_2]/dt = 2.5-2.0$ mmol/h under the Standard Conditions. As we will see later, the induction period and slope correlate linearly with the rate constants k_1 and k_2 obtained from curvefitting (*vide infra*), so that measurement of the induction period and of $-d[H_2]/dt$ is a fast yet quantitative way to evaluate individual kinetic runs. Reproducibility of the induction period or hydrogenation rate (slope) is typically ±10% within the same batch of acetone, cyclohexene *and* precatalyst, and ±20% between batches.

In all the studies to follow (and as seen before),[20] the reaction solutions turned deep blue before the end of the cyclohexene hydrogenation run. The color is due to H_2 reduction of the polyoxoanion's W^{VI} sites ("spillover of H• ")[20a] to yield a reduced form of the polyoxoanion, **2**, one containing one or more W^{V}•−W^{VI} mixed-valence pairs. Such blue solutions subsequently turn brown (the normal $Ir(0)_{\sim 300}$ nanocluster color) within minutes after opening the Fischer-Porter bottle back inside the N_2 drybox, a phenomenon that is apparently due the well-established (re)evolution of H_2 ("reverse spillover").[2b,20a] This follow-up or side reaction is of little consequence to the present studies focused on the mechanism of $Ir(0)_{\sim 300}$ nanocluster formation, and hence need not be mentioned further herein. It is, however, of interest as the first good molecular mimic of the phenomenon of H_2 spillover that is important in heterogeneous catalysis, and for this reason it has been discussed more elsewhere.[2b]

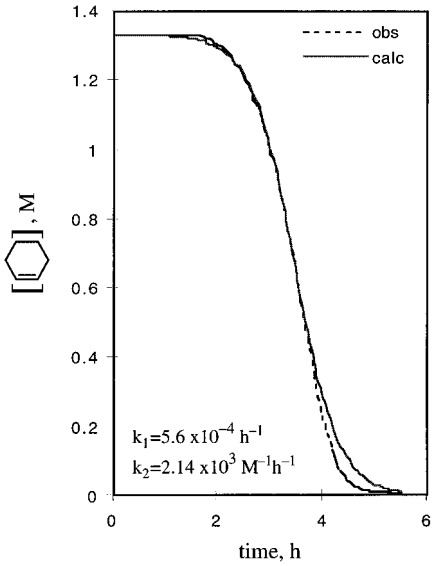

Figure 3. Typical curvefit of the loss of cyclohexene demonstrating the excellent fit to the nucleation plus autocatalysis, then hydrogenation, three step kinetic model in eqs 2a−c. The resultant rate constant k_2 has been corrected by the mathematically required scaling factor.[46]

Curvefits: Nucleation Plus Autocatalytic Growth. Figure 3 shows a typical curvefit of cyclohexene uptake during the hydrogenation reaction with **1** as precatalyst and under our Standard Conditions. Although the loss of H_2 pressure is monitored experimentally via the computer-interfaced, ±0.01 psig pressure transducer (i.e., as in Figure 2 above), the equivalent (1:1) *cyclohexene loss* will be used hereafter for the curvefits, largely because of its generally more useful units of molarity. Note that one must not confuse here the origins of the stoichiometry of the measured H_2 loss: it has nothing to do (to three significant figures) with the nonintegral, 300 **1** to 750 H_2 nanocluster formation stoichiometry shown back in Scheme 1. Instead, the *stoichiometry* of the H_2 loss is due to the reaction of 1 cyclohexene + 1 H_2 to give 1 cyclohexane. This is true, by design, since the ratio of cyclohexene to **1** is ca. 1400−1 under our Standard Conditions. *However*, the *kinetics* of the H_2 loss do follow the nanocluster formation as proved below; this is the beauty of the indirect but powerful method of following the kinetics developed herein and while employing the concept of pseudoelementary mechanistic steps, *vide infra*.

The first result to note is that the fits are excellent according to the simple, three step, nucleation, autocatalysis and[34] then hydrogenation steps in eqs 2a−c below—a remarkable result considering that the reaction must consist of a *minimum* of ≥300 steps [i.e., given that the average reaction stoichiometry shown back in Scheme 1 involves 300 **1** + 750 H_2 to give 1 $Ir(0)_{\sim 300}$ (+ 300 cyclooctane + 150 H^+ and 300 $P_2W_{15}Nb_3O_{62}^{9-}$)]. Hence, the three step minimum mechanistic scheme found to

(33) See pp 109−111 elsewhere.[31]

fit the data is a ≥100-fold reduction in complexity! It follows that the majority of the reaction steps must be fast, but that the fits have identified the slow, crucial rate-determining steps. It is also logical to infer that the present multistep nanocluster "self-assembly" reaction uses one key step repetitively. That step is the key autocatalytic surface-growth step examined next.

The second result of note is that *only* if an autocatalytic step, A + B → 2B, specifically eq 2b, is included, can one then come even close to fitting the curves observed such as that in Figure 3. This is a result we demonstrated previously using numerical integration methods,[35] and a result that is intuitive as well in that we both (a) know of no other kinetic function which will allow a reaction to sit seemingly "dormant" for 2 h but then go to completion in an additional 2 h, a total of 4 h, Figure 3, nor (b) were we able to find such a function empirically.[35] The k_1 and k_2 values[32] that result from the curve fit are, in turn, used in conjunction with eq 4 to compute the calculated curve (the solid line) also shown in Figure 3. Note that the fit to this unusually shaped kinetic curve is excellent (i.e., throughout all but the very last parts of the curve; that too is understood and will be discussed later), *quantitative* results which provide very strong support for autocatalysis.

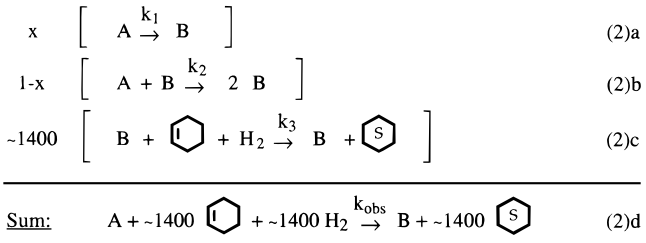

where A is the precatalyst, $[Bu_4N]_5Na_3[(1,5\text{-COD})Ir{\cdot}P_2W_{15}Nb_3O_{62}]$, and B is the catalyst (the active Ir(0) surface sites on the near-monodisperse distribution of nanoclusters present); that is, eqs 2a−c become 2a′−c′:

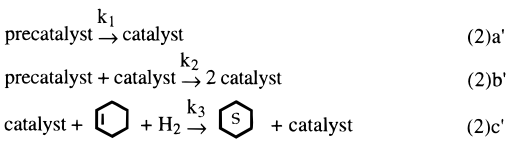

A key but perhaps not immediately obvious point is that the excellent curvefit in Figure 3 requires that the third step, 2c, be fast in comparison to the first two steps, 2a and 2b. This key point is developed more in the next section. Note also that implicit in the kinetic treatment above is the assumption that all Ir(0) atoms on the surface of the developing, different size (as a function of time) nanoclusters react at the same rate. To ensure that this is the case as much as possible, hydrogenation was deliberately chosen for these initial studies since it is the classic so-called "structure-insensitive" (i.e., largely particle-size insensitive) reaction, at least after a critical size nucleus, $Ir(0)_n$, is formed that is metastable and can activate H_2 (see the references and additional discussion of structure-insensitivity and of why we chose hydrogenation, discussion provided previously on p 4904 and in footnote 52 elsewhere[20b]). We will return later, in the Discussion, to the issue of whether or not a particle size dependence is involved in the observed sigmoidal-shaped hydrogenation curves.

The Pseudoelementary Kinetic Model. A bit of reflection reveals what **A** and **B** must correspond to in our system: a look at eq 2c reveals that **B** is, by definition, the hydrogenation catalyst(s). Previously, we provided compelling evidence that the range of nanoclusters represented by $Ir(0)_{\sim 300}$ (plus the smaller, still forming nanoclusters) are the active hydrogenation catalysts formed from **1** under H_2—that is, the nanocluster surface Ir(0) active sites are the catalyst, **B**.[20b] The identity of **A** is, then, obvious: it must be the precatalyst, **1**. Reflection also reveals why we were able to follow the hydrogenation reaction, eq 2c, yet see the kinetics of autocatalysis (i.e., the shape of the curve in Figure 2), and thus why we were able to learn about the desired $Ir(0)_{\sim 300}$ nanocluster formation reaction, steps 2a and 2b. The necessary concept here is that of a *pseudoelementary mechanistic step*,[29] a term invented by a former colleague at the University of Oregon, Professor Richard Noyes, for dealing with complex (oscillating) reactions. As the results herein also show, it is likely to become a standard concept when one deals with more complex kinetic and mechanistic schemes (i.e., with the mechanistic complexity that promises to be a significant part of the future of mechanistic science).

A consideration of eq 2d, the reaction obtained by summing the three steps outlined in eqs 2a−c, reveals the concept of a pseudoelementary step as used in the present example. If the third step, 2c, is fast on the time scale of the first and second steps, then it follows that the kinetics of the overall reaction, 2d, will be those of steps 1 and 2 only. In addition, since the H_2-consuming reactants (cyclohexene) in the third step are in a 1400-fold higher concentration than the H_2-consuming reactants in the first and second steps, the overall H_2 consumption *stoichiometry* is given by the net reaction, 2d, but is due (to better than three significant figures) to only the third step, 2c. Hence, by following the concentration changes of the third step, we can follow the nanocluster formation reaction *and its kinetics*.

It should now be clear that step 2d can be treated and used kinetically as equivalent to an elementary step, even though step 2d is obviously not elementary (i.e., it is composed of *at least* the three steps shown). Reaction 2d is an illustrative example of what Noyes has termed *pseudo*elementary.[29]

The applicable rate equation[36] for the kinetically important steps 2a and 2b is shown in eq 3 (see the discussion available in a footnote[32] and the derivation in the Appendix for the equations which follow):

$$-\mathrm{d[A]}/\mathrm{d}t = +\mathrm{d[B]}/\mathrm{d}t = k_1[\mathrm{A}] + k_2[\mathrm{A}][\mathrm{B}] \qquad (3)$$

The following analytical expression results, eq 4:

$$[\mathrm{A}]_t = \frac{\frac{k_1}{k_2} + [\mathrm{A}]_0}{1 + \frac{k_1}{k_2[\mathrm{A}]_0} * \exp(k_1 + k_2[\mathrm{A}]_0)t} \qquad (4)$$

Values of the rate constants k_1 and k_2 can in fact be obtained readily from the slope and intercept of a linearized form of eq 4 (in the limit that $k_1 \ll k_2[\mathrm{A}]_0$ and $[\mathrm{A}] < [\mathrm{A}]_0$),[36] but the k_1 and k_2 values so derived are less precise and, therefore,

(34) The following provide a general initial reference to autocatalysis,[34a] plus key papers in the autocatalysis literature describing polymerization (polyimide synthesis),[36] formaldehyde condensation into sugars assisted by Ca^{2+} and HO^-,[34b] sickle hemoglobin aggregation,[34c] plus a review of biological pattern formation involving autocatalysis.[34d] (a) Steinfeld, J. I.; Fransisco, J. S.; Hase, W. L. *Chemical Kinetics and Dynamics*; Prentice Hall: NJ, 1989. (b) Heidmann, W.; Decker, P.; Pohlmann, R. *Origins of Life* **1978**, 625−630. (c) Ferrone, F. A.; Hofrichter, J.; Eaton, W. A. *J. Mol. Biol.* **1985**, *183*, 611. (d) Grierer, A. *Prog. Biophys. Mol. Biol.* **1981**, *37*, 1−47.

(35) Lyon, D. K.; Finke, R. G. *Inorg. Chem.* **1990**, *29*, 1784.

(36) Kaas, R. L. *J. Polym. Sci. Polym. Chem. Ed.* **1981**, *19*, 2255.

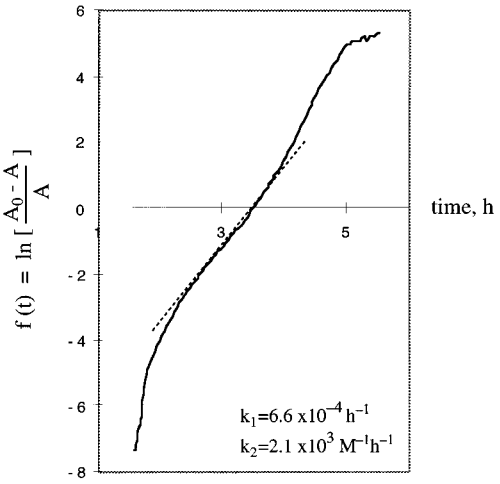

Figure 4. Linearized plot of the loss of cyclohexene. This curve was generated from the identical data used to generate Figure 3 and thus compares directly the two ways to analyze the kinetic data.

presumably also less accurate.

$$f(t) = \ln\left[\frac{[A]_0 - [A]}{[A]}\right] = \ln\left[\frac{k_1}{k_2[A]_0}\right] + k_2[A]_0 t \qquad (5)$$

Figure 4 is a plot of the same experimental points as in Figure 3 but linearized via eq 5. The fact that the plot deviates from linearity at short times is due to deviations from the assumption $[A] < [A]_0$ which is necessary for the derivation of eq 5. The deviations at longer times are due to the fact that step 2c is no longer fast on the time scale of steps 2a and 2b at the end of the reaction where the concentration of cyclohexene approaches zero—that is, due to the failure of the reaction 2d to be pseudoelementary at longer times.

Correlation of Calculated Rate Constants with the Observed Induction Periods and $-d[H_2]/dt$ Slopes. As shown in Figure 5a, a linear correlation is observed between the *inverse* of the induction period obtained manually and the k_1 values obtained by curve-fitting the identical curves. A linear correlation is also observed when the hydrogenation rate, $-d[H_2]/dt$, obtained manually is plotted against the curve-fit-obtained k_2, Figure 5b. Therefore, one can rapidly extract quantitative induction-period or hydrogenation rate data manually from any given run (e.g., as in Figures 2 or 3).

A Control Testing the Pseudoelementary Model: Demonstration of a Zero-Order Cyclohexene Concentration Dependence. The pseudoelementary model in eqs 2a−d makes one key kinetic prediction that can be readily tested: the cyclohexene concentration should be zero order under at least higher cyclohexene concentration conditions which allow step 2c to be fast. This was tested, and the results are shown in Figure 6. Increasing the initial cyclohexene concentration has no effect on the k_1 value (or, equivalently and as actually plotted in Figure 6a, on the manually obtained induction period). The k_2 value, on the other hand (or, equivalently and as actually plotted in Figure 6b, the hydrogenation rate, $-d[H_2]/dt$), reaches a zeroth-order dependence above *ca.* 1.5 M, that is, exhibits "saturation kinetics". Since we work with initial cyclohexene concentrations of 1.65 ± 0.10 M, we are working where the observed induction period ($\alpha(1/k_1)$) and hydrogenation rate (α-(k_2)) are independent of the cyclohexene concentration. These observations confirm that the third step, eq 2c, is fast relative to 2a and 2b and thus that *the pseudoelementary treatment is indeed valid*. As desired, step 2c simply magnifies and reports, but does not influence, the kinetics of steps 2a and 2b. In simpler terms, while monitoring the hydrogenation catalysis stoichiometry, we are actually learning, as desired, about the nanocluster formation kinetics.

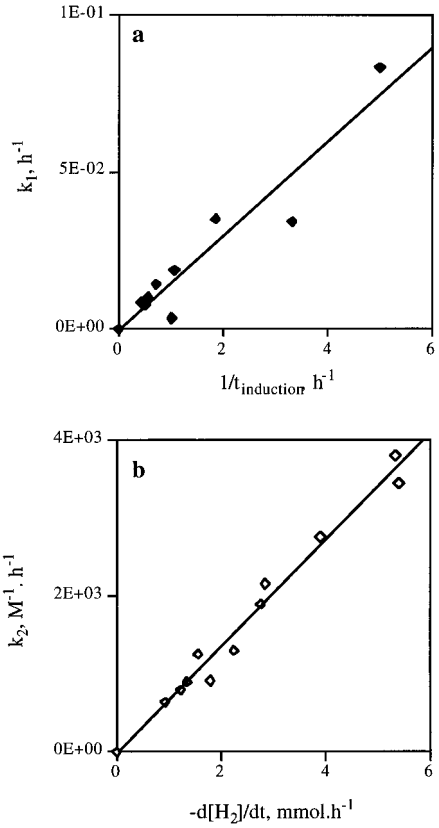

Figure 5. Correlation between the induction periods and $-d[H_2]/dt$ slopes with the curvefit values of, respectively, k_1 and k_2. (These particular data are taken from our earlier work,[20b] data which were, however, curvefit for the first time herein using eqs 2a−c.)

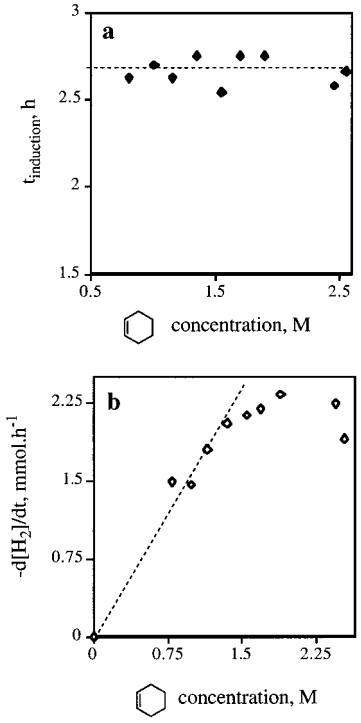

Figure 6. Effect of cyclohexene concentration on the hydrogenation induction period and rate. While the dotted line fits the data in Figure 6a, the dotted line in Figure 6b is included simply to show the change from an apparent first- to the expected zero-order dependence upon olefin.

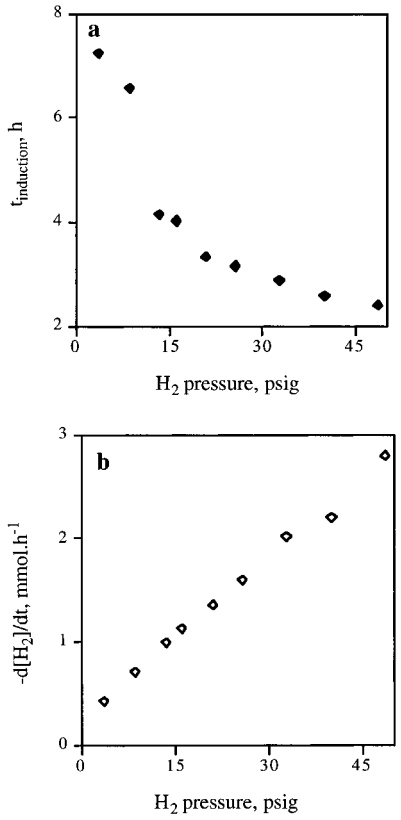

Figure 7. Effect of the initial hydrogen pressure on the induction period and the $-d[H_2]/dt$ hydrogenation rate. [The "zero" data point, i.e., the assumed zero hydrogenation rate at zero (−14.7 psig) hydrogen pressure, is not shown since we expect our mechanism to no longer be obeyed at low H_2 pressures (where, for instance, nanoparticle aggregation is already known to become competitive at even 1 atm H_2).[20a]]

We can now interpret with confidence the observation that the calculated data points reach larger values than the experimental ones toward the end of the reaction shown back in Figure 3. This is just an artifact introduced when the conditions required for the pseudoelementary model are no longer satisfied, specifically the cyclohexene concentration approaching zero late in a hydrogenation reaction. Under these conditions, the hydrogenation step 2c is no longer fast relative to steps 2a and 2b, and thus the key assumption of the pseudoelementary model—that step 2c is fast—is no longer valid. In fact, we previously showed that the timescale of catalyst formation is ca. 1.3-fold longer than that of cyclohexene reduction (see Figure 7 elsewhere),[20b] so that the first and second steps (eqs 2a,b) and thus nanocluster growth are still taking place when the hydrogenation reaction, eq 2c, has run completely out of cyclohexene (but while there is still ca. 24 psig of H_2 pressure remaining as Figure 2, for example, illustrates). From the cyclooctane evolution data we know that only ca. 75 ± 5% of the cyclooctane has evolved when the cyclohexene reduction is complete, corresponding to the formation of, *on average*, ca. $Ir_{230\pm15}$ nanoclusters at that time.

Effect of Initial Hydrogen Pressure. The results in Figure 7 show that with increasing initial hydrogen pressure the induction period *decreases* in a nonlinear fashion, but that the $-d[H_2]/dt$ rate *increases* and does so linearly. Indeed, for the first and second reaction steps, eqs 2a and 2b, a first-order dependence on hydrogen pressure was expected. Hence, we can now rewrite step 2a as A + H_2 → B and step 2b as A + B + H_2 → 2B, so that the rate equation, eq 3 for example, becomes $d[B]/dt = k_1[A][H_2] + k_2[A][B][H_2]$. Under our conditions, H_2 is in very large excess relative to A and, to the extent that H_2 is constant, then the rate equation simplifies to $d[B]/dt = k_{1obs}[A] + k_{2obs}[A][B]$, where k_{1obs} and k_{2obs} are pseudo-first- and -second-order rate constants, respectively.[37]

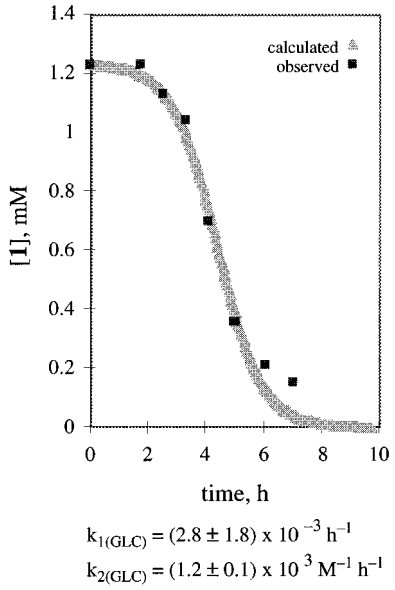

Figure 8. Loss of the precursor $[Bu_4N]_5Na_3[(1,5\text{-COD})Ir{\cdot}P_2W_{15}Nb_3O_{62}]$, **1**, as monitored by its GLC-determined evolution of 1.0 equiv of cyclooctane.

The observations in Figure 7 of a H_2-dependence to steps 2a and 2b are again fully consistent with and supportive of our finding that steps 2a and 2b but not the third reaction, step 2c, are controlling the kinetics of the $Ir(0)_{\sim300}$ nanocluster-forming reaction.

One Additional Key Control: Demonstration That Direct Monitoring of the $Ir(0)_n$ Nanocluster Formation Reaction via Its Evolution of Cyclooctane Yields the Same Rate Constants, k_1 and k_2. It is important to check our kinetic method by a more direct way of monitoring the Ir(0) nanocluster formation. Fortunately, the well-defined precursor, $[Bu_4N]_5Na_3[(1,5\text{-COD})Ir{\cdot}P_2W_{15}Nb_3O_{62}]$, **1**, has one additional, very valuable handle: the Ir(0) formation can be monitored directly by the cyclooctane evolution that accompanies the conversion of the precursor, **1**, into Ir(0) nanoclusters under H_2. The loss of **1** as measured by its 1:1 cyclooctane evolution stoichiometry (see the established stoichiometry[20a,b] reproduced in Scheme 2)-should show an autocatalytic shape, and it should yield the same rate constants, within experimental error, after curve-fitting to the identical equations used to analyze the hydrogenation curves.

The loss of **1** determined by the GLC evolution of cyclooctane, Figure 8, is sigmoidal, is well-fit by the same eqs (2a and 2b, and their associated eq 4), and yields the same rate constants within experimental error as those obtained from following the hydrogenation in this same run and after application of the mathematically required correction factors,[38] $k_{1(GLC)} = 2.8\ (\pm1.8) \times 10^{-3}$ h^{-1}; $k_{2(GLC)corrected} = 2.3\ (\pm0.2) \times 10^{3}$ M^{-1} h^{-1} compared to $k_{1(hydrogenation)} = 1.8\ (\pm0.2) \times 10^{-3}$ h^{-1} and $k_{2(hydrogenation)corrected} = 2.5\ (\pm0.3) \times 10^{3}$ M^{-1} h^{-1}. The large error bar on the GLC-derived k_1 rate constant is due to the fewer—and much lower precision—data available by the GLC

(37) Note, however, that while H_2 is in a large excess, it is not constant. Instead, it decreases from a maximum of 40 psig to ca. 32 psig during the time in which data are used for a curvefit (the data from the ca. first half of a standard hydrogenation curve, Figure 2). But, in a practical sense the hydrogen pressure can be taken as a "constant" 36 ± 4 psig over the time when kinetic data is taken; this introduces a quite tolerable error of only ca. ±11% into the final k_1 and k_2 values.

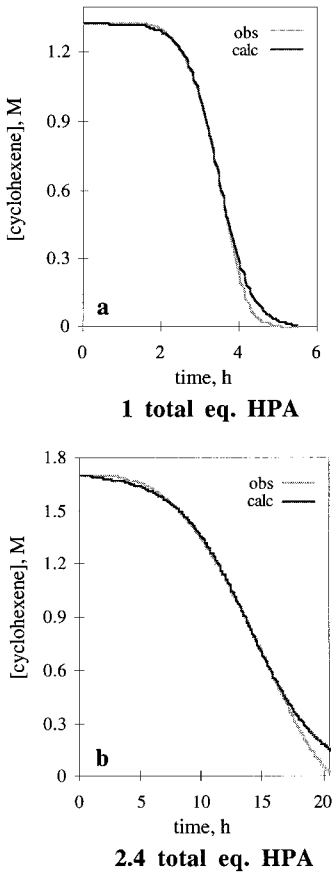

Figure 9. Effect of added heteropolyoxoanion (HPA), $[Bu_4N]_9[P_2W_{15}Nb_3O_{62}]$, **2**; typical curve-fits.

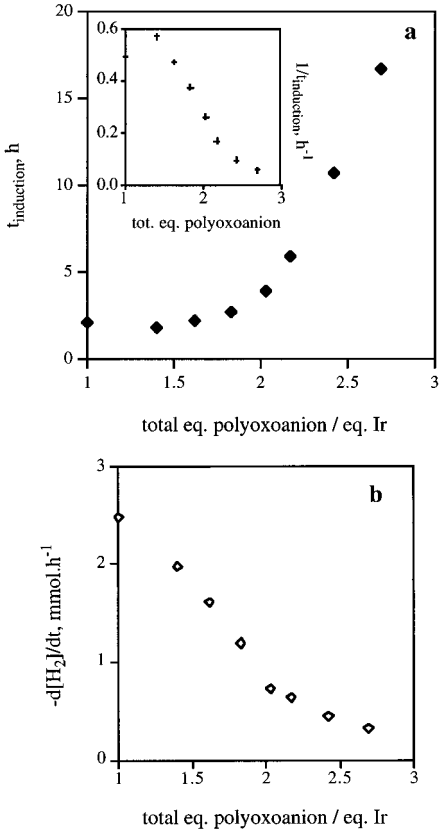

Figure 10. Effect of added polyoxoanion on the induction period and hydrogenation rate. The inset in Figure 10a shows the inverse plot of $1/t_{induction}$ vs total equiv of added polyoxoanion.

method compared to the hydrogenation method (i.e., and its continuous stream of ±0.01 psig pressure transducer-obtained data). The important result is that the identical resultant k_1 and k_2 values offer *compelling evidence that the two methods are monitoring the same process*, $Ir(0)_n$ nanocluster formation.

Typical Curvefits as a Function of Key Additives. Typical curvefits of the loss of cyclohexene under Standard Conditions, but *plus* the additives noted with each figure, are given in Figure 9 (added polyoxoanion), Figure S-1, Supporting Information (added water), Figure S-2, Supporting Information (added acetic acid), and Figure S-3, Supporting Information (the effect of varying the reaction temperature). In general the curvefits are excellent during at least the first half of the reaction. However, in the cases of added water (Figure S-1-b) or added acetic acid (Figure S-2-b), the calculated (curvefit) points deviate from the experimental points during the latter half of the reaction. While there are several possible *a priori* explanations for this, nanocluster agglomeration (leading to a significant decrease in the catalytic surface and thus an experimentally slowed reaction) is an obvious reason that comes to mind. In studies in progress, we are attempting to (a) verify by TEM this proposed aggregation step, and, if correct, then (b) study the kinetics of the putative nanocluster aggregation step(s).

Quantitative Studies of Nanocluster Formation as a Function of Key Additives: Observed Rates and Induction Periods. Effect of Added Polyoxoanion. As shown in Figure 10a, the induction period increases with added equiv of the $[Bu_4N]_9[P_2W_{15}Nb_3O_{62}]$ polyoxoanion, **2**, approaching infinity above 2.7 total equiv of **2** (i.e., the hydrogen uptake rate approaches the background (i.e., minimum) value of 0.05 psig/2.5 min or 0.325 mmol/h at 22 °C with which we define the induction period). This is excellent evidence for a small prior equilibrium, $K_{diss} \ll 1$, as part of the nucleation step(s), one that the inverse $[P_2W_{15}Nb_3O_{62}^{9-}]$ dependence indicates must involve the dissociation of a $[P_2W_{15}Nb_3O_{62}]^{9-}$ fragment from the precatalyst, $(1,5\text{-COD})Ir(P_2W_{15}Nb_3O_{62})^{8-}$, **1**, and thus must involve the release of a $[Ir(1,5\text{-COD})(solvent)_x]^+$ fragment. Just such a step will be presented as part of our more detailed mechanistic proposal, Scheme 3 (*vide infra*).

On the other hand, Figure 10b shows that the hydrogenation rate decreases with added polyoxoanion. While a fuller discussion of this result (as well as of the other results to follow) is delayed until the Discussion section, the data would seem to demand that the added polyoxoanion in some way cover parts of the Ir(0) nanocluster surface, thereby either blocking access to, or otherwise inhibiting the catalytic reactions of, the catalytically active Ir(0) surface. As such, the data in Figure 10b is another piece of evidence[20a] *indicating that the polyoxoanions are close to and interacting with the Ir(0) nanocluster's surface*.

Effect of Added Water. As shown in Figure 11a, the hydrogenation induction period decreases with added equiv of water to ca. 0.15 h, that is, effectively zero, since this is the

(38) (a) Note that the mathematics require that the hydrogenation curvefit k_2 (i.e., $k_{2(hydrogenation)}$) is corrected by a stoichiometry factor,[32] $k_{2(hydrogenation)} = 1400k_{2(fit)}$. (b) Both $k_{2(hydrogenation)}$ and $k_{2(GLC)}$ are corrected by a scaling factor, $x_{average}$,[46] introduced by the changing number of surface to total Ir(0) atoms (see the derivations in Appendix C and footnote 46): $k_{2(hydrogenation)corrected} = k_{2(hydrogenation)}/0.72$ and $k_{2(GLC)} = k_{2(GLC)corrected}/0.51$. Note that the scaling factors are different since the GLC method, for example, follows the Ir(0) formation over a different part and fraction of the nanocluster growth than does the hydrogenation method. (c) Note also that these values k_1 and k_2 should not be compared to the raw k_1 and k_2 values in Figures 3 and 4, for example, since that data are uncorrected as done above,[38b] and also were obtained with a different batch of precursor **1** and H_2O-containing acetone, both of which are known to influence the observed kinetic results (see also the data as a function of the acetone source, the amount of H_2O and the other results presented elsewhere[20b] and also in Figure 11 herein).

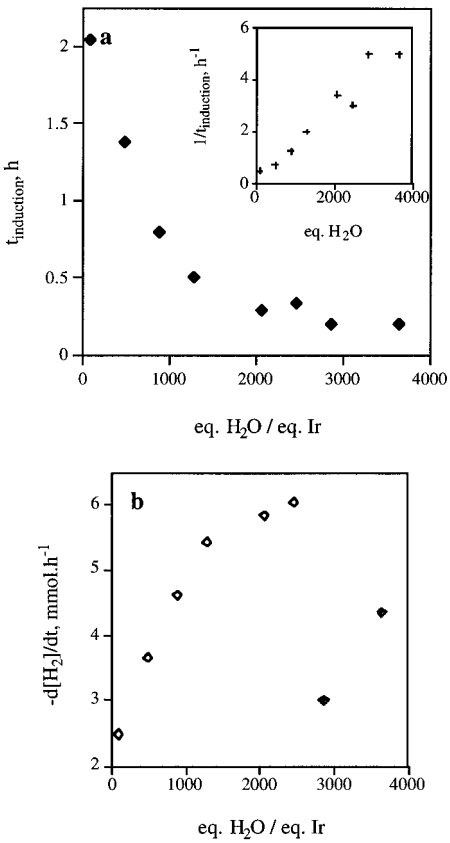

Figure 11. Effect of added water on the induction period and hydrogenation rate. The inset in Figure 11a shows the inverse plot of $1/t_{induction}$ vs total equiv of added H_2O.

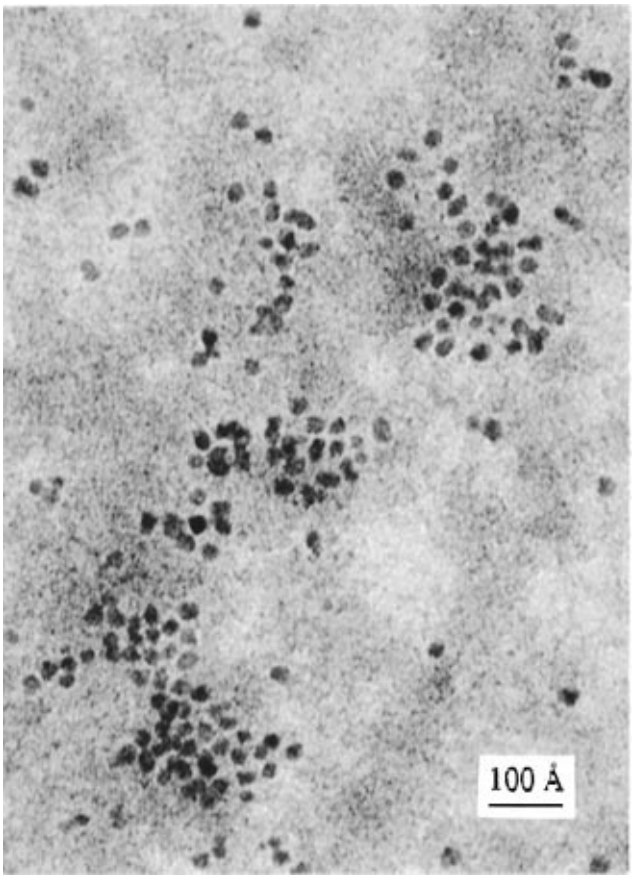

Figure 12. TEM of a fresh acetonitrile solution of iridium(0) clusters synthesized under Standard Conditions (magnification: 430 K). The results show that the iridium(0) clusters are well dispersed.

minimum value measurable experimentally and, hence, used to signal the end of the induction period. On the other hand, the hydrogenation rate initially increases with added equiv of water, reaching a maximum value of 6.0 mmol/h, but then becoming highly variable above 2500 equiv, a variability with high [H_2O] that we previously showed[20b] is due to the formation of a low, variable surface area (and thus lower and variable catalytic activity) bulk Ir(0) metal precipitate. (Black insoluble material, confirmed to be $Ir(0)_{bulk}$ as detailed in the Experimental Section, deposits in the test tube by the end of the hydrogenation run. In runs in which smaller amounts of water are added, one also observes the formation of a black insoluble deposit, but only following several days to weeks of standing.)

The effect of added H_2O is not a trivial observation in that it reveals the ability of H_2O to *destabilize* organic-solvent-soluble nanoclusters. The exact destabilization reaction is not yet known, but the most plausible reaction is the protonation of the basic polyoxoanion, $P_2W_{15}Nb_3O_{62}^{9-} + H_2O \rightarrow HP_2W_{15}Nb_3O_{62}^{8-} + OH^-$. This would have the effect of removing the nanocluster-stabilizing[20a] $P_2W_{15}Nb_3O_{62}^{9-}$ and replacing it with OH^-, a ligand that we previously demonstrated is less stabilizing than the polyoxoanion.[20a]

Effect of Added Acetic Acid. As shown in Figure S-4 of the Supporting Information, the effect of added dry acetic acid on the hydrogenation induction period and rate looks qualitatively very similar to that of added water (recall Figure 11). With dry HOAc, the induction period quickly reaches a minimum value of 0.37 h, and the rate a maximum value of 4.7 mmol/h. When the solutions were kept for several days or weeks, black insoluble $Ir(0)_{bulk}$ is deposited. These results suggest that HOAc, and probably H_2O as well have, achieve their observed effects due to their *acidity*. This postulate is strongly supported by our earlier observation that added Na^+OAc^- has no measurable effect on either the induction period or the hydrogenation rate.[20b]

Effect of Temperature. Lastly, Figure S-5 (Supporting Information) shows that, as one might expect, the induction period decreases with increasing temperature, reaching a minimum value of 0.33 h, while the hydrogenation rate increases to a maximum value of 8.2 mmol/h; that is, normal, positive temperature dependencies are seen. The usual ln (k) vs $1/T$ plots provide apparent (i.e., composite) activation parameters for these respective, composite k_1 and k_2 steps of $\Delta H_1^{\ddagger} = 15 \pm 1$ kcal/mol and $\Delta S_1^{\ddagger} = -36 \pm 3$ eu and $\Delta H_2^{\ddagger} = 14 \pm 2$ kcal/mol and $\Delta S_2^{\ddagger} = -13 \pm 6$ eu (1 M standard state). Since these values are composites for multiple elementary steps, they are of course primarily useful only to calculate the temperature dependence of these two, again composite, steps. However, it is worth noting that these activation parameters (i) predict a relatively small temperature dependence to the $k_2 \cdot [B]/k_1$ ratio (and thus relatively small size changes as a function of temperature,[24] *vide infra*) and (ii) demonstrate the difference between the present system vs literature systems that are purported to follow the *little verified* suggestion that $\Delta H^{\ddagger}_{nucleation}$ ought to be $\gg \Delta H^{\ddagger}_{growth}$.[11a]

The important insight now available is that one can now easily calculate how the *ratio* of $k_2 \cdot [B]/k_1$ varies with temperature. This is significant since it is this ratio which contains information on how to control nanocluster sizes. In fact, the topic of the $k_2 \cdot [B]/k_1$ ratio is important enough that it is the focus of a separate paper.[24]

TEM Analyses. Figure 12 shows a typical TEM of the $Ir(0)_{\sim 300}$ clusters prepared from the precatalyst **1** and under the Standard Conditions detailed in the Experimental Section. The image shown was obtained via a dry sample sent for TEM and

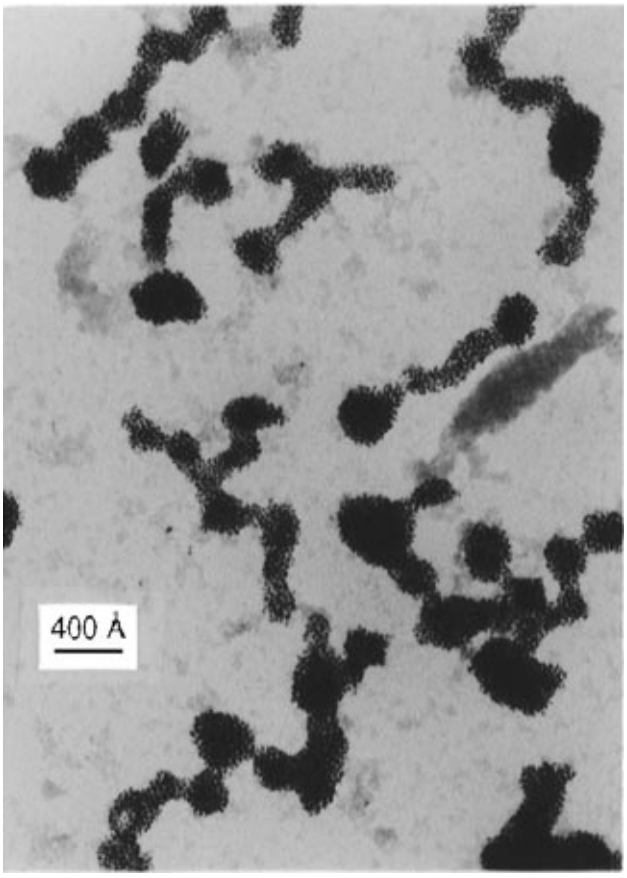

Figure 13. TEM of a 6 week old acetonitrile solution of iridium(0) clusters synthesized under Standard Conditions (magnification: 100 K). The results reveal that the iridium(0) clusters have agglomerated.

then redispersed in acetonitrile solution just before the TEM analysis (see the Experimental Section). The TEM confirms the previously reported[20] uniformity in size and shape, and the well dispersed nature, of the $Ir(0)_{\sim 300}$ nanoclusters.

Figure 13, on the other hand, gives a TEM representation of a sample prepared under the exact same Standard Conditions, but in which the acetonitrile solution was prepared 6 weeks before the actual TEM analysis (and then shipped via the mail to Oregon where the TEMs were obtained; see the Experimental Section). While there is still uniformity in size and shape of the individual clusters, they do show considerable agglomeration, indicating that the storage of samples dry, followed by the preparation of fresh solutions just before TEM analyses, is the preferred method of TEM sample handling for at least these $Ir(0)_{\sim 300}$ nanoclusters.

TEMs for the samples prepared under the range of experimental conditions and additives are given in Figures S-6−S-9 of the Supporting Information along with histograms detailing the Ir(0) nanocluster diameters. Those images reveal that the ±2 Å resolution of normal TEM does not allow us to make quantitative statements about the trends in size or the size distribution, since differences of ca. 5 Å correspond to the addition of each new shell of Ir(0) atoms. To detect such differences reliably, we need and plan to turn to high-resolution (HR) TEM studies.

Discussion

A Consideration of Alternative Explanations for the Sigmoidal Shape of the Observed Hydrogenation and Cyclooctane Evolution Curves. It is crucial in science in general, and mechanism in particular, that one remembers that one can only disprove alternative hypotheses and mechanisms, thereby offering evidence consistent with any remaining mechanisms. Hence, it is important at this point, and before going further, to consider any conceivable alternative explanations for the observed sigmoidal cyclooctane evolution and hydrogenation progress curves—do any exist, and if so, can they be disproven? The only even conceivable explanation that we could come up with is summarized by the question: could a particle-size dependence *alone* give rise to the sigmoidal curves seen? We were able to rule out this conceivable possibility based on six lines of evidence, the details of which are provided in the Supporting Information. The most compelling four of the six lines of evidence are (i) first and foremost, it is both physically and mathematically unreasonable that the analytic function in eq 4—which was derived from autocatalysis as the growth pathway and which fits the sigmoidal curves quantitatively—can simultaneously be the correct *analytic* function, and at all time values, for both autocatalysis and, separately but simultaneously, for the putative particle-size explanation; (ii) second, the expected effect of particle-size *alone* is a rate decrease, not increase, for two reasons: the percentage of Ir(0) atoms on the surface decreases with particle size[46c] and the intrinsic reactivity probably also *decreases* with particle size due to the greater thermodynamic stability of larger particles;[10,44] and (iii) third, the comparison of the (sigmoidal) cyclooctane and (sigmoidal) hydrogenation curves reveals that they are quantitatively connected by the *mathematically predicted* stoichiometric factor of $k_2 = 1400k_2$(fit). In the particle size-dependence explanation, some as-of-yet-unavailable *ad hoc* explanation would be required here. Fourth, (iv) it is not at all clear how the observed zero-

(39) See Figure 9 p 110 of Che, M.; Bennett, C. O. *Adv. Catal.* **1989**, *36*, 55−172. Note that Figure 9 therein of ethylene hydrogenation rate vs particle size is zero below 2.5 Å, shows a maximum at ca. 6 Å, and then decreases to 1/3 the maximum and to a roughly constant rate after a 10 Å Pt particle size (i.e., shows a "volcano plot"). But, within this factor of 3 the ethylene hydrogenation reaction is so-called "structure-insensitive". Note also that since a support (SiO_2) is present, one cannot rule out, on these data alone, an effect as a function of particle size by the SiO_2 on the hydrogenation rate (i.e., rather than some intrinsic rate effect due to the metal particle size alone).

(40) The basic features of this mechanism were proposed by us in 1994,[20a] but only now is (a) compelling kinetic evidence available to support this scheme and (b) can alternative mechanisms be ruled out such as discrete homogeneous catalysts (once believed in the literature to be the only way to account for such reproducible kinetic data, an only recently disproved notion[20b]).

(41) Collman, J. P.; Hegedus, L. S.; Norton, J. R.; Finke, R. G. *Principles and Applications of Organotransition Metal Chemistry*; University Science Books: Mill Valley, CA, 1987; Chapter 5.

(42) (a) K_{diss} is too small to be directly observed with, for example, no dissociated (1,5-COD)Ir(acetone)$_2^+$ or $P_2W_{15}Nb_3O_{62}^{9-}$ being detectable by ^{1}H NMR or ^{31}P NMR, respectively. (b) However, a *crude* estimate of the value of K_{diss} can be obtained from the curvature of the plot $t_{induction}$ vs {1/added equiv of polyoxoanion} as follows: the quantity $t_{induction}$ is proportional to $1/k_1$ (see Figure 6), which in turn should be proportional to 1/[(1,5-COD)Ir(acetone)$_2^+$] (= 1/*y*, by definition). At the low levels of (1,5-COD)Ir(acetone)$_2^+$ dissociation implied by its nondetectability, 1/*y* is in turn proportional to {[added eq polyoxoanion]/K_{diss}}. Hence, the curvature of the experimental plot of $t_{induction}$ vs {1/added equiv of polyoxoanion} was compared to the curvature generated by calculated 1/*y* vs {1/added equiv of polyoxoanion} and for a range of different K_{diss} values. The closest, *rough* match was found with $K_{diss} \leq 10^{-4}$, as the figure below shows.

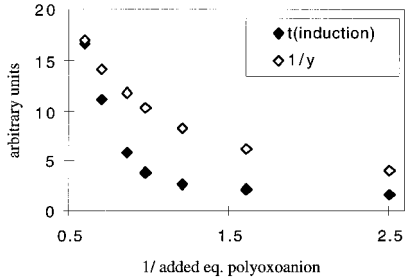

order [cyclohexene] dependence (recall the top of Figure 6, main text) would be rationalized under the particle-size explanation. Other evidence against a particle-size-effect *alone* as the correct explanation for the sigmoidal shape of the kinetic curves is presented in the Supporting Information.

Note that we do believe the observed induction period is in fact just the time required to form the critical $Ir(0)_n$ nucleus. Consistent with this, we know from the cyclooctane evolution data that only $Ir(0)_{\sim 70\pm 20}$ nanoclusters have formed even after half the cyclohexene hydrogenation uptake is complete in a Standard Conditions run, Figure 3. In addition, it is already established in the literature that a small, critical particle size is required for the fastest ethylene hydrogenation activity (ca. 6 Å for Pt on SiO_2).[39] Hence, it is an integral part of our proposed mechanism that no hydrogenation catalysis occurs until after a small, critical size $Ir(0)_n$ nucleus is reached during the induction period. In addition, *we fully expect a small particle-size dependence may be hidden in the observed k_2 values.* Two reasons for saying this are (a) such a small but intrinsic size-dependence to the true k_2 for olefin hydrogenation is expected, and (b) it is probably possible to build in mathematically a small size dependence to k_2 (i.e., atop the basic autocatalysis and sigmoidal curve shape) exactly analogous to how we added on a "scaling factor" correction for the number of surface to total Ir(0) atoms, *vide infra*.

Proposed, More Detailed Nanocluster Formation Mechanism. Scheme 3 provides a more detailed, but still deliberately minimal, mechanistic description of the formation of $Ir(0)_{\sim 300}$ nanoclusters during the hydrogenation of **1** and cyclohexene in acetone.[40] It is worth emphasizing that we know that our nanocluster formation reaction is under *kinetic control* since elevated temperatures and longer times result in conversion of the nanoclusters to the thermodynamic sink of bulk Ir(0) metal.[2b,20b]

Scheme 3. A *Minimum Mechanism* for the Formation of Ir(0) Nanoclusters: (i) Slow, Continuous Nucleation, Followed by (ii) Fast, Autocatalytic Surface Growth

$$(1,5\text{-COD})Ir(P_2W_{15}Nb_3O_{62})^{8-}\ (\mathbf{1}) + 2\ \text{acetone} \rightleftharpoons (1,5\text{-COD})Ir(\text{acetone})_2^{+} + P_2W_{15}Nb_3O_{62}^{9-} \quad (I)$$

$$(1,5\text{-COD})Ir(\text{acetone})_2^{+} + 2.5\ H_2 \rightarrow \bigcirc + Ir(0) + H^{+} \quad (II)$$

$$n\ Ir(0) \rightarrow Ir(0)_n \quad (III)$$

$$\mathbf{1} + 2.5\ H_2 + Ir(0)_n \rightarrow \bigcirc + Ir(0)_{n+1} + H^{+} + P_2W_{15}Nb_3O_{62}^{9-} \quad (IV)$$

The basic features of this proposed mechanism and the main supporting evidence for each step are as follows. The five-coordinate, d^8 Ir(I) precursor complex **1** cannot activate hydrogen directly because of its 18 electron, full-shell electron configuration.[41] In addition, the increase in the induction period with added $P_2W_{15}Nb_3O_{62}^{9-}$, Figure 10, implicates a prior K_{diss} that is $\ll 1$[42] in which **1** dissociates $P_2W_{15}Nb_3O_{62}^{9-}$ and, by mass balance, $[Ir(1,5\text{-COD})^{+}]$. Hence, reduction of Ir(I) to Ir(0) by H_2 is proposed to take place by steps I and II via the known, solvated, 16 electron complex[27c] $Ir(1,5\text{-COD})(acetone)_2^{+}$ (that differs from the analogous $Ir(1,5\text{-COD})(solvent)_2^{+}$ complex employed in the synthesis of **1** only in that solvent = acetone rather than acetonitrile).[27,28] Step II, the rapid reduction of $(1,5\text{-COD})Ir(acetone)_2^{+}$ to Ir(0) metal is known to occur essentially immediately under H_2.[20a] In addition, steps I and II explain the induction-period decreasing effects of H^{+} (HOAc or the weaker acid H_2O) via protonation of the $P_2W_{15}Nb_3O_{62}^{9-}$, thereby shifting the equilibrium in step I to the right and resulting in a dramatically shorter induction period (recall Figure 11a and see also Figure S-4-a; recall also that a control reaction[20b] showed that OAc^{-} had no effect, i.e., that the effect of HOAc is due to its H^{+}).

As Ir(0) atoms are *slowly and continuously generated* via step II, they undergo aggregation to the critical nucleus size, $Ir(0)_n$, step III. The sum of steps I−III provides homogeneous nucleation.[43] Note that such an Ir(0) agglomeration step is necessary given that we start with the *single* Ir(I)-containing complex **1** but end up with a complex with 300 Ir(0) atoms on the average, $Ir(0)_{\sim 300}$. There is an enthalpic driving force[10] to the Ir(0) aggregation step (i.e., once the high energy Ir(0) atoms have been formed); one can estimate that each Ir(0)−Ir(0) bond formed is worth ca. 26 kcal/mol on the average. (Recall that Ir(0) in bulk Ir(0) metal has six such Ir−Ir bonds for a total stabilization, vs Ir(0) atoms, of 159 kcal/mol.)[44] However, there is an enthalpy *cost*[10] to be paid due to the work (surface tension) of creating two phases (solute and solvent) as the nanocluster grows. The entropy loss accompanying aggregation opposes this step, but a critical nucleus is attained when the additional Ir(0)−Ir(0) bonds possible in a "larger" $Ir(0)_n$ particle overtake the combination of the entropy loss and the surface tension enthalpy increase so that the critical nucleus, $Ir(0)_n$, becomes stable toward dissociation into Ir(0) fragments. Computations (for Pt clusters) suggest that even Ir_4 to Ir_{13}, for example, may be of sufficient size to form a critical nucleus.[19b,44b] In fact, for the cyclooctane evolution data already published in Figure 7 elsewhere[20b] we know that ≤5% of **1** has evolved to Ir(0) by the end of the induction period, *a result which places an upper limit on the average critical nucleus size of* $\leq Ir(0)_{\sim 15}$. Previous experimental determinations of a transition metal nanocluster critical-nucleus size are virtually unknown.

(43) (a) Our kinetic evidence detailed in the main text requires a nucleation step which is unimolecular in the precatalyst, **1**; this, in turn, implies nucleation via single Ir(0) atom formation. Given the available thermochemical considerations,[10,45] we expect that even single Ir(0) atoms up to the critical nucleus $Ir(0)_n$ are stabilized by bonding to the $P_2W_{15}Nb_3O_{62}^{9-}$ polyoxoanion, or possibly the olefin (cyclohexene), even though this is not specifically shown in Scheme 3. (b) Previously, we provided evidence for homogeneous nucleation by demonstrating that an increase in the glass surface area (using added glass beads) does not affect the induction period.[20b] This result was verified as part of the present studies, as we showed that a 2.5-fold increase in the glass surface area (using added glass beads) made no detectable change in an otherwise Standard Conditions hydrogenation reaction and k_1 and k_2 values. Such *evidence against any detectable component of heterogeneous nucleation* is necessary since heterogeneous nucleation can often be a faster, lower energy pathway,[43c] at least in nanocluster formation reactions proceeding by diffusion−controlled pathways. (c) A key paper in the homogeneous, diffusion-controlled nucleation literature: Strey, R.; Wagner, P. E.; Viisanen, Y. *J. Phys. Chem.* **1994**, *98*, 7748. We thank Prof D. Johnson, University of Oregon, for bringing this paper to our attention and for his critical commentary on the topic of nucleation. (d) One can envisage a continuous nucleation process, one thermodynamically more favorable than isolated Ir(0) formation, involving more than one Ir(0)—possibly in a bi- or trimetallic precursor, thereby gaining the stability associated with Ir−Ir bond formation.[10] However, we know of no evidence in the nanocluster or colloid literature for such a process, at least to date, although it is an interesting target for future research. (e) Growth at step and kink sites on surfaces: Burton, W. K.; Cabrera, N. *Discuss. Faraday Soc.* No. 5, **1949**, 33−48. See, also classic review: Burton, W. K.; Cabrera, N.; Frank, F. C. *Trans. Roy. Soc. (London)* **1951**, *A243*, 299−358.

(44) (a) The $\Delta H_{vaporization}$ of bulk Ir(0) metal is 159 kcal/mol (see footnote 47 elsewhere[20a]). This in turn means that 12-coordinate Ir(0) in the bulk solid experiences an average bond energy of 159/(12/2) = 26 kcal/mol (12/2 since it takes two Ir atoms to form one Ir−Ir bond). This back-of-the-envelope analysis reveals the high driving force especially for Ir(0) atoms, and also for $Ir(0)_x$ nanoparticles, to aggregate to the thermodynamically favored, low-surface-area, Ir(0)−Ir(0) bonded form (and, ultimately, to bulk Ir(0)). This calculation also teaches that nanocluster and colloid stabilization is, at least to date for transition metal nanoclusters, a totally kinetic phenomenon. (b) See elsewhere for papers discussing the energetics[16,19] or structures[18] accompanying particle growth. (c) Estimation of the Ir(0)−Ir(0) BDE as done above[44a] is common, see: Conner, J. A. *Topics Curr. Chem.* **1977**, *71*, 71, see Table 3, p 78. Pichler, G.; Skinner, H. A. In *The Chemistry of the Metal−Carbon Bond*; Hartley, F. R., Patai, S., Eds.; John Wiley: New York, 1982; see p 78, Table 13.

Once the critical nucleus, $Ir(0)_{\leq 15}$, is formed it is able to catalytically effect the direct reduction of **1**, that is, of [(1,5-COD)Ir^{I}]$^{+}$ still attached to the polyoxoanion.[45] This is the autocatalytic step demanded by the compelling kinetic evidence for autocatalysis presented herein. In the present case each new Ir(0) atom is added to the surface of an existing $Ir(0)_n$ nanocluster, that is $Ir(0)_n + Ir(0) \rightarrow Ir(0)_{n+1}$, step IV—the key being that the $Ir(0)_{n+1}$ product of the reaction is also a catalyst for that very same reaction, thereby producing autocatalysis. There is, however, a different "scaling" type correction factor to our autocatalytic step; specifically, the *fraction* of active surface atoms gained in $Ir(0)_n \rightarrow Ir(0)_{n+1}$ is not exactly 1 as in 1B $\rightarrow$ 2B back in step 2b but instead is the difference $[Ir(0)_{n+1(\text{surface atoms})} - Ir(0)_{n(\text{surface atoms})}]$. This simply introduces a scaling factor, x, to the rate constant k_2 obtained, but in no way invalidates or otherwise changes the kinetic fits. Hence, the interested reader is directed to a footnote[46] and the Appendix for a further discussion of this detail. Note also that the literature indicates that the Ir(0) reduction and hence initial growth sites on non-full shell (i.e., non-magic number) nanoclusters are likely at the nanocluster surface step and kink sites.[43e]

The fact that the autocatalysis is a *surface*-growth reaction (rather than a LaMer mechanism with diffusion-controlled addition of high-energy Ir(0) atoms to the $Ir(0)_n$ surface) follows from three lines of evidence: (i) first, the autocatalysis makes no sense if it involves high-energy Ir(0) formation in solution (i.e., there is no reasonable, alternative way to effect the reduction of polyoxoanion-coordinated Ir(I) that would, in such an alternative hypothesis, have to be somewhere in solution, far from the $Ir(0)_n$ surface where H_2 is activated); (ii) second, there is a good—albeit a single—precedent for the *surface*-growth nature of such reactions, namely Whitesides' work on (1,5-COD)PtR_2 reduction under H_2 to form a heterogeneous $Pt(0)_nR_2$ catalyst. (However, the focus of that work is the organic products and their stereochemistry; hence, unstudied are the topics most relevant to the present work, i.e., the metal Pt(0) product, its characterization, nor is there any kinetic evidence for the mechanism of Pt(0) production[47]). Third, and perhaps most compellingly, (iii) any Ir(0) atoms produced in solution are roughly m·26 kcal/mol higher in energy than when bound to $Ir(0)_n$ as in $Ir(0)_{n+1}$ (where m = the number of Ir(0)−Ir(0) bonds made upon forming $Ir(0)_{n+1}$ from $Ir(0)_n$)—a number that is likely $\geq$78 kcal/mol![48] Indeed, it is amazing that one can form sufficient Ir(0) atoms to nucleate the autocatalytic surface-growth process in the first place, even with the ca. 2 h induction period.

The reduction process in the *catalyzed* step IV is kinetically much faster than that in the uncatalyzed steps I and II, a point that is apparent qualitatively by the sigmoidal shape of the hydrogenation curves presented. Quantitatively, the ratio of the rates of the catalyzed to the uncatalyzed reactions, $k_2[B]/k_1$, is 2.5×10^3.[49] It is not at all surprising, then, that once $Ir(0)_n$ nuclei are formed in solution, the generation of Ir(0) by surface autocatalytic growth kinetically dominates further slow—but still continuous—nucleation via steps I−III. The important consequence of autocatalytic surface-growth is that it *separates nucleation and growth in time*, the end result of which is the observed near-monodisperse, $\leq \pm 15\%$ size distribution.[20b]

Not shown as part of Scheme 3 are the post rate-determining steps of nanocluster aggregation and "Ostwald Ripening",[13a] steps that are known to be universal in nanocluster and colloid science.[13e] However, we have (a) written them down previously (step V of Scheme 2 elsewhere)[20a] but (b) only see evidence for them under conditions different than those studied herein (i.e., notably at low H_2 pressure). Hence, those results will be reported as part of a separate study.[23]

Overall, then, there is excellent if not compelling evidence for each step in the minimum mechanism depicted in Scheme 3. The main issues that remain to be discussed herein are (a) any further analysis of, and insights from, the kinetic data, especially on the key autocatalytic step and its rate constant, k_2, and (b) the literature evidence for or against the broader applicability of the present nucleation and surface autocatalytic-growth mechanism—does it apply broadly to other nanocluster syntheses *using H_2 as a reducing agent?*

Additional Analysis and Insights from the Kinetic Data. The Effect of the Various Additives upon the Autocatalytic Step and Its Rate Constant, k_2. Not discussed yet are why added $P_2W_{15}Nb_3O_{62}^{9-}$ polyoxoanion, H_2O, or H^+ produce the changes seen in the autocatalytic step and its rate constant, k_2, that is, the decrease with added polyoxoanion (Figure 10), the increase with added H_2O (Figure 11), and the increase with added H^+ (Figure S-4). The rate decreasing effect of added polyoxoanion on k_2 suggests a blockage of the $Ir(0)_{\sim 300}$ nanocluster surface (i.e., more so than the Nb−O−Nb bridged, anhydride form of the polyoxoanion that is normally present),[20b] thereby slowing one or more steps of the cyclohexene hydrogenation reaction. Significantly, these data (Figure 10) provide additional evidence for the polyoxoanion coordinating to, and thereby stabilizing,[20a] the nanocluster.

The effect of added HOAc was established to be an H^+, and not a OAc^-, effect. We have obtained evidence that the effect of H^+ on k_2 is via a little precedented H^+-assisted reductive-elimination step in the $Ir(0)_{\sim 300}$ nanocluster catalyzed hydrogenation reaction, and those results will be reported separately in due course.[50] Analogous H^+-assisted reductive-elimination reactions almost surely also occur in heterogeneous catalysis, as it explains, for example, why protic solvents like EtOH or HOAc are often preferred in heterogeneous hydrogenations.[51]

(45) Unfortunately, attempts to measure by cyclic voltammetry a potential of the Ir(I)/Ir(0) redox couple of the supported polyoxoanion complex, [(1,5-COD)Ir·$P_2W_{15}Nb_3O_{62}$]$^{8-}$, failed to show any peaks (in CH_3CN, at a Pt electrode).

(46) (a) As explained in more detail in Appendix C, the steps of nucleation (nIr(0) $\rightarrow$ $Ir(0)_n$) and growth ($Ir(0)_n$ + "Ir(0)" $\rightarrow$ $Ir(0)_{n+1}$) can be summarized by "2A $\rightarrow$ $(1 + x_{\text{growth}})$B", where x_{growth} is the fraction of active surface atoms gained in the growth step. The value of x_{growth} is thus given by the ratio of the increase in the number of surface atoms divided by the increase in the total number of atoms. (b) As detailed in Appendix C, the rate equation for "2A $\rightarrow$ $(1 + x_{\text{growth}})$B" is given by $-d[A]/dt = k_1[A] + k_2((1 + x_{\text{growth}})/2)[A]([A]_0 - [A])$. The calculated value of k_2 (obtained from curvefitting, then corrected by the stoichiometry factor)[32] is thus really $k_{2(\text{calculated})} = k_2((1 + x_{\text{growth}})/2)$. This becomes relevant when comparing values of $k_{2(\text{calculated})}$ in which values of the "scaling factor" ($x = (1 + x_{\text{growth}})/2$) vary. (c) An average value of the factor x_{growth} can be calculated for the addition of one atomic shell to a full-shell nanocluster (the formula for the number of atoms added to the nth shell of a nanocluster is $10n^2 + 2$, see: Teo, B. K.; Sloane, N. J. A. *Inorg. Chem.* **1985**, *24*, 4545). Alternatively, $x_{\text{average}} = (1 + \text{no. surface atoms})/(1 + \text{total no. atoms})$ can be defined and used:

shell no.	no. surface atoms	total no. atoms	x_{growth}	x_{average}
1→2	12→42	13→55	0.71	0.72
2→3	42→92	55→147	0.54	0.60
3→4	92→162	147→309	0.43	0.51

For curvefitting purposes, only the data prior to the consumption of half the initial cyclohexene concentration was included (see the Experimental Section). At that time only 23 ± 7% of the initial amount of Ir(I) has been reduced to Ir(0) (i.e., only 23 ± 7% of the total equivalent of cyclooctane has evolved, see Figure 7 elsewhere),[20b] indicating that the average cluster size is probably 70 ± 20 atoms. There the value of the factor x_{growth} is close to 0.7.

(47) (a) McCarthy, T. J.; Shih, Y.-S.; Whitesides, G. M. *Proc. Natl. Acad. Sci. U.S.A.* **1981**, *78*, 4649. (b) Whitesides, G. M.; Hackett, M.; Brainard, R. L.; LaVelleye, J. P.-P.; Sowinski, A. F.; Izumi, A. N.; Moore, S. S.; Brown, D. W.; Staudt, E. M. *Organometallics* **1985**, *4*, 1819. (c) Miller, T. M.; Izumi, A. N.; Shih, Y.-S.; Whitesides, G. M. *J. Am. Chem. Soc.* **1988**, *110*, 3146. (d) Lee, T. R.; Whitesides, G. M. *Acc. Chem. Res.* **1992**, *25*, 266 and references therein to the other papers in this series.

We presume that one effect of added H_2O is just this H^+ effect, an interpretation consistent with the fact that it takes ca. 1000 equiv of the weaker acid H_2O to have the same ca. 2-fold rate enhancing effect seen for 10 equiv of HOAc (compare Figures 11 and S-4). The fact that the maximum increase for water (vs no added water) is 2.5-fold, and thus greater than the 1.9-fold maximum effect of HOAc (vs no added HOAc), *may* indicate some additional, smaller effect is also present for H_2O (although the differences are marginally larger than the propagated experimental error).

Literature Suggesting the Broad Applicability of the Autocatalytic Surface-Growth Mechanism for Nanoclusters Synthesized under H_2. A search of the literature reveals many nanocluster syntheses under H_2 which, when those papers are reread in light of the mechanism presented herein, suggest that those syntheses also proceed via the basic features of the mechanism deduced herein. For example, Whitesides and co-workers[47] report, in their studies of hydrogenation of (diolefin)-(dialkyl)Pt(II) complexes (catalyzed by Pt(0) black), that (i) the final mass of Pt(0) catalyst increases proportionally to the amount of Pt(II) complex reduced and (ii) in the absence of Pt(0) catalyst, the reaction proceeds after an *induction period* and results in the formation of (colloidal and bulk) Pt(0). Blum and co-workers,[52a] during their study of olefin hydrogenation in the presence of a Rh(III) precatalyst, report key observations which point toward our mechanism (even though the presence of Rh(0) was not acknowledged), specifically: (i) an induction period for olefin hydrogenation is observed unless the Rh(III) complex is pretreated with H_2 and (ii) black insoluble particle formation is observed unless additional (stabilizing) tertiary amine is added. In work that will be published elsewhere we have shown that the Blum and co-workers system in fact produces Rh(0) nanoclusters and that those nanoclusters are the active catalyst instead of the claimed, monometallic complex, $R_3R'N^+RhCl_4^-$.[52b]

Many additional preparations of metal colloids or clusters by H_2 reduction of a metal ion—including the first $R_4N^+Cl^-$ stabilized colloid[53] —are reported in the literature, and there is every reason to believe that these obey the autocatalytic surface-growth mechanism elucidated herein.[54−60] In some instances, thermodynamically favored structures such as magic number[61,62] or surfactant-stabilized, shape-controlled clusters[15] are obtained. These observations point to our mechanism as well since (i) magic number clusters are a natural consequence of a surface-growth mechanism as we detail elsewhere[24] and (ii) shape-control by capping ligands is a natural consequence of surface-growth, where weakly or uncapped surfaces will grow faster than tightly ligand-capped surfaces. This latter implication of our mechanism, while preliminary and thus still requiring testing, begins to fill the void noted by others, that "... the mechanism for the nucleation and growth of shape-controlled nanoparticles has not been determined" (see p 1163 elsewhere).[15a] It is also likely that nanocluster syntheses involving H_2 reduction of the *ligand* in a M(0) complex also obey this same mechanism. Evidence consistent with this statement includes the previously unexplained induction periods seen prior to colloid formation.[63]

Furthermore, we have recent evidence[64] that our mechanism is even more general if one allows for variations in the initial (reductive) nucleation steps, for example, when the mechanism of initial H_2 activation is no longer *cis*-oxidative addition[41] but where the *autocatalytic surface-growth step* remains the same. Those observations, which will also be reported in due course,[64] again employ the autocatalytic surface-growth step and, hence, argue further for its broad applicability in nanocluster syntheses employing H_2 as the reducing agent.

Predictions of the Autocatalytic Surface Growth Mechanism Remaining To Be Tested. A significant feature of the mechanism herein is that it makes key predictions, via the autocatalytic surface-growth, eq 2b ($A + B \rightarrow 2B$) and step IV, that remain to be tested and verified or refuted. Specifically, it predicts (i) that magic number nanoclusters[21,24] will tend to be formed when this mechanism operates, simply because full shell nanoclusters are more stable thermodynamically and, therefore, should tend to grow slower kinetically; (ii) that nanoclusters like $Ir(0)_{\sim 300}$ are "living metal polymers" so that one can achieve size-control using smaller "seeds" [65] to synthesize larger nanoclusters, especially those with magic number sizes; and (iii) that one can grow sequentially, from "nanoseeds" (call them B), higher bi-, tri-, and higher-*multimetallic* nanoclusters[65b] of *known, initial, "onion-skin" structure* (e.g., via $B + C \rightarrow B/C$, then $D + B/C \rightarrow B/C/D$, where C and D are metals able to activate H_2 and which grow on the surface

(48) This back-of-the-envelope calculation makes the crude assumption that a surface Ir(0) is, *on the average*, six-coordinate and thus will experience roughly 1/2 of the final 159 kcal/mol of Ir−Ir bonding energy it would feel if it were bulk, ccp, 12 coordinate $Ir(0)_n$ metal. (The coordination number of surface Ir(0) actually varies from 3 to 9.) This calculation also ignores any Ir(0) solvent coordination bond energy that would have to be overcome, and thus would decrease the amount of energy released when the Ir(0) atoms combine.

(49) In the calculation of $k_2[B]/k_1$: (a) the value of [B] was taken as the average concentration of active surface Ir(0) sites, [B] = (number Ir_{300} clusters)·(number surface atoms in Ir_{300}) = ([**1**]/300)·162. This yields [B] = 6.4×10^{-4} M. (b) The value of k_2 was corrected by the stoichiometry factor $[\text{cyclohexene}]_0/[\mathbf{1}]_0$.[32] (c) No attempt was made to correct the value of k_2 by the scaling factor x.[46]

(50) (a) Müller, F.; Aiken, J. D., III; Lyon, D. K.; Finke, R. G. Unpublished results. (b) What we find striking here is that, even in this first nanocluster reaction mechanism study from our labs[23] and one studying catalysis' arguably best studied reaction, hydrogenation,[51] we have *already* found a little−appreciated elementary step, H^+-assisted reductive-elimination. This mechanistic finding also bodes well for future catalytic reaction and mechanistic studies using well−defined, relatively stable nanoclusters.

(51) (a) Augustine, R. L.; Yaghmaie, F.; Van Peppen, J. F. *J. Org. Chem.* **1984**, *49*, 1865. (b) Philipson, J. J.; Burwell, R. L., Jr. *J. Am. Chem. Soc.* **1970**, *92*, 6125. (c) Horiuti, I.; Polanyi, M. *Trans. Faraday Soc.* **1934**, *30*, 1164.

(52) (a) Blum, J.; Amer, I.; Vollhardt, K. P. C.; Schwarz, H.; Höhne, G. *J. Org. Chem.* **1987**, *52*, 2804. (b) Weddle, K. S.; Aiken, J. D., III; Finke, R. G. Submitted for publication.

(53) Kiwi, J. Grätzel, M. *J. Am. Chem. Soc.* **1979**, *101*, 7214.

(54) (a) Bönnemann, H.; Brinkmann, R.; Köppler, R.; Neiteler, P.; Richter, J. *Adv. Mater.* **1992**, *4*, 804. (b) Bönnemann, H.; Brijoux, W.; Brinkmann, R.; Fretze, R.; Joussen, T.; Köppler, R.; Korall, B.; Neiteler, P.; Richter, J. *J. Mol. Catal.* **1994**, *86*, 129. Reported therein is that Pd(0), formed initially from R_3BH^- reduction of Pd^{2+}, catalyzes further nanocluster growth by reducing (probably autocatalytically) additional Pd^{2+} using H_2 (see p 155). (c) Review: Bönnemann, H.; Brijoux, W. In Active Metals; Fürstner, A., Ed.; VCH Publishers: New York, 1996; Chapter 9, pp 339−397. Note on p 361 the use of H_2 as a preferred reducing agent.

(55) Rampino, L. D.; Nord, F. F. *J. Am. Chem. Soc.* **1942**, *63*, 2745.

(56) Henglein, A.; Ershov, B. G.; Malow, M. *J. Phys. Chem.* **1995**, *99*, 14129.

(57) Toshima, N.; Takahashi, T. *Bull. Chem. Soc. Jpn.* **1992**, *65*, 400.

(58) Boutonnet, M.; Kizling, J.; Stenius, P.; Maire, G. *Colloids Surfaces* **1982**, *5*, 209.

(59) Harrison, J. B.; Berkheiser, V. E.; Erdos, G. W. *J. Catal.* **1988**, *112*, 126.

(60) Yonezawa, T.; Tominaga, T.; Richard, D. *J. Chem. Soc., Dalton Trans.* **1996**, 783.

(61) Vargaftik, M. N.; Zagorodnikov, V. P.; Stolarov, I. P.; Moiseev, I. I.; Kochubey, D. I.; Likholobov, V. A.; Chuvilin, A. L.; Zamaraev, K. I. *J. Mol. Catal.* **1989**, *53*, 315.

(62) (a) Schmid, G.; Morun, B.; Malm, J.-O. *Angew. Chem., Int. Ed. Engl.* **1989**, *28*, 778. (b) Schmid, G.; Harms, M.; Malm, J.-O.; Bovin, J.-O.; Van Ruitenbeck, J.; Zandbergen, H. W.; Fu, W. T. *J. Am. Chem. Soc.* **1993**, *115*, 2046. (c) Schmid, G.; Maihack, V.; Lantermann, F.; Peschel, S. *J. Chem. Soc., Dalton Trans.* **1996**, 589.

(63) (a) Bradley, J. S.; Millar, J. M.; Hill, E. W.; Behal, S.; Chaudret, B.; Duteil, A. *Faraday Discuss.* **1991**, *92*, 255. (b) Bradley, J. S. In *Clusters and Colloids. From Theory to Applications*; Schmid, G., Ed.; VCH: New York, 1994; p 459.

(64) Widegren, J. A.; Weddle, K. S.; Watzky, M. A.; Finke, R. G. Unpublished results and experiments in progress on the kinetics and mechanism of nanocluster formation under H_2 of different metals.

of B to yield B/C, and then on the surface of B/C to yield B/C/D). The existence of 1906 as well as 1996 literature that uses seed growth methods to make bimetallic nanoclusters[65c] is further evidence for the broad generality of the mechanism presented here—especially its autocatalytic surface-growth step. *However, unrecognized until now is that autocatalysis and surface growth are almost surely occurring and that at least the initial stucture of these nanoclusters should favor an onion-skin motif.* The autocatalytic surface growth mechanism further predicts (iv) that capping ligands[14,15] that are face selective can be exploited to grow nanoclusters that have different, possibly even predesigned shapes, (v) that there will likely be variations in the basic mechanism we have discovered (evidence already is forthcoming that variations exist due to initial mechanisms of H_2 activation other than *cis* oxidative-addition[64] and due to H_2 mass-transfer limitations[23]); and (vi) that the autocatalytic surface-growth step is likely to be more general even beyond H_2 as the reductant, probably extending to cases such as citrate,[11] BH_3,[14] and any other reductants where the reductant is activated faster on the surface of the metal than with the precatalyst (e.g., possibly HCO_2H, N_2H_4, CO/H_2O, and other sources of "H_2"; all of these are under investigation). This will especially be true—and can be used as a design feature—when an 18 electron, coordinatively saturated complex is selected as the precatalyst. One final prediction of the autocatalytic surface growth mechanism is (vii) that it should be applicable to the formation of supported metal-particle heterogeneous catalysts[65] or thin films under hydrogen. Consistent with this, Kaesz and co-workers[66] report an induction period for a thin metallic film deposition (by CVD, using a Pt(II) precursor complex under H_2) in the absence of a previously formed film. However, if a thin Pt(0) film is preformed, the H_2 reduction of further Pt(II) proceeds without an induction period, very likely via an autocatalytic surface-growth mechanism. Also noteworthy is that in all cases, the autocatalytic surface growth mechanism should show a preference toward near-monodispersed ($\leq \pm 15\%$) size distributions, since autocatalysis separates nucleation and growth in time.

To summarize, the autocatalytic surface-growth mechanism contains many predictions of and insights for how to grow a myriad of size-, shape-, and multimetallic-composition-controlled nanoparticles. Such particles would be ones where the size, shape, and metal in a given dimension are controlled, at least ideally, by the use of seeds, different metals (in controlled amounts and controlled orders of addition), plus capping ligands selective to certain metal faces (and, in some syntheses, their removal at a preselected time in the synthesis, so that the capping ligands serve as metal-face-selective "protecting groups"). *In short, it is the principle of autocatalytic surface-growth that is the most significant and more general finding herein.* We look forward to seeing its application and exploitation tested in the designed syntheses of new size, shape, and composition transition metal nanoclusters.

(65) (a) Professor G. Schmid points out in his recent layered Au/Pd publication[65b] that the "seed" or "germ" based syntheses of nanoclusters has been known since 1906[65c] (see also the other relevant references provided therein). (b) Schmid, G.; West, H.; Malm, J.-O.; Bovin, J.-O.; Grenthe, C. *Chem. Eur. J.* **1996**, *2*, 147. (c) Michel, J. B.; Schwartz, J. Y. In *Catalyst Preparation Science*; Delmon, B., Grange, P., Jacobs, P. A., Poncelet, G., Eds.; Elsiever, New York, 1987; Vol. IV, pp 669−687. (d) Ketelson, H. A.; Brook, M. A.; Pelton, R.; Heng, Y. M. *Chem. Mater.* **1996**, *8*, 2196. Figure 2 therein rather convincingly demonstrates that Ag(0) is grown atop supported Pt particles, by what must be a surface-growth mechanism, from Ag^+ and hydroquinone as the reducing agent. (e) Che, M.; Cheng, Z. X.; Louis, C. *J. Am. Chem. Soc.* **1995**, *117*, 2008. That work reports evidence for a silica-attached Ni(II) nucleation site, plus surface growth (and subsequent particle agglomeration) from impregnated, weakly adsorbed Ni(II), when the system is *reduced with* H_2. The mechanistic work provided in the present paper suggests that these authors' unproved postulate (p 2018), that the surface growth is on *Ni(II)*, should be replaced by surface growth on *Ni(0)*. In addition, it is unclear if the surface growth is (either Ni(II) or Ni(0)) diffusion limited or autocatalytic.

(66) (a) Chen, Y.-J.; Kaesz, H. D.; Thridandam, H.; Hicks, R. F. *Appl. Phys. Lett.* **1988**, 1591. (b) Xue, Z.; Strouse, M. J.; Shuh, D. K.; Knobler, C. B.; Kaesz, H. D.; Hicks, R. F.; Williams, R. S. *J. Am. Chem. Soc.* **1989**, *111*, 8779. (c) Klabunde has discussed the nucleation and diffusive-growth stages in metal-atom depositions yielding thin metal films: Davis, S. C.; Klabunde, K. J. *Chem. Rev.* **1982**, *82*, 153.

Summary and Conclusions

In this study, the first kinetic and mechanistic study of the formation of modern, compositionally well-defined, and highly catalytically active nanoclusters—ones which promise to serve as prototype "soluble heterogeneous catalysts"[2b]—we have

(1) developed an indirect—but easy, continuous, highly quantitative and thus powerful—method to monitor the formation of the $Ir(0)_{\sim 300}$ nanoclusters via their catalytic hydrogenation activity and through the concept of pseudoelementary reaction steps;

(2) applied the appropriate kinetic equations for nucleation and autocatalysis and then demonstrated that these equations fit the observed, sigmoidal-shaped kinetic curves *quantitatively* with resultant rate constants k_1 and k_2;

(3) confirmed by the more direct method of monitoring the Ir(0) formation via its cyclooctane evolution that the method in (1) indeed works and does so quantitatively, yielding the same k_1 and k_2 values within experimental error;

(4) collected a wealth of previously unavailable kinetic and mechanistic data on nanocluster formation, under the often preferred reductant H_2, of the effects of added olefin, H_2, anionic nanocluster stabilizer ($[Bu_4N]_9P_2W_{15}Nb_3O_{62}$ in the present case), H_2O, HOAc, and temperature;

(5) carefully considered and been able to rule out the alternative mechanistic hypotheses that particle size rate effects *alone* are the reason for the observed, sigmoidal shaped curves (although we fully expect that a particle-size effect remains to be deconvoluted out of k_1 and k_2);

(6) distilled the results into a minimalistic mechanism consisting of two key, rate-controlling, psuedoelementary steps: (i) slow, continuous nucleation, followed by (ii) fast, autocatalytic surface-growth;

(7) presented a concise but comprehensive review of the literature of transition metal nanocluster formation under H_2 as the reducing agent, an analysis which provides *highly suggestive evidence* that the new mechanism uncovered is a much more general *mechanistic paradigm for transition metal nanoclusters formed under* H_2 *and related reducing agents;* and

(8) summarized the key predictions of this new mechanism which remain to be tested.

Overall, it is hoped that the results—the first new mechanism in more than 45 years for transition metal nanocluster formation—will go far toward providing a firmer mechanistic basis, and perhaps even a new paradigm, for the designed synthesis of new transition metal nanoclusters of prechosen sizes, shapes, and mono- to multimetallic compositions.

Acknowledgment. The TEMs in this work were obtained with the expert assistance of Dr. Eric Schabtach at the University of Oregon's Microscopy Center. Jody Aiken is acknowledged for his valuable technical assistance. Two anonymous referees are thanked for their comments that helped sharpen the presentation of this lengthy contribution. Financial support was provided by the Department of Energy, Chemical Sciences Division, Office of Basic Energy, Grant DOE FG06-089ER13998.

Appendix A: Pseudoelementary Step Treatment of the Kinetics

Recall that we use a pseudoelementary step to follow the production of $[B]_t$, via its (magnified) catalytic hydrogenation of cyclohexene. As usual, one must start the kinetic derivation with the rate-determining steps, k_1 and k_2:

$$\text{A.1}\quad \frac{-\mathrm{d}[A]}{\mathrm{d}t} = \frac{+\mathrm{d}[B]}{\mathrm{d}t} = k_1[A] + k_2[A][B] = k_1[A] + k_2[A]([A]_0 - [A])$$

(by the mass balance equation, $[B] = [A]_0 - [A]$).

Next, we need to turn this into what we actually follow. This must be done via the stoichiometry of the pseudoelementary step

$$\text{A.2(a)}\quad \frac{1}{1}\frac{-\mathrm{d}[A]}{\mathrm{d}t} = \frac{1}{1}\frac{+\mathrm{d}[B]}{\mathrm{d}t} = \frac{1}{\sim 1400}\frac{-\mathrm{d}[\bigcirc]}{\mathrm{d}t} = \frac{1}{\sim 1400}\frac{-\mathrm{d}[H_2]}{\mathrm{d}t}$$

$$\text{A.2(b)}\quad \frac{-\mathrm{d}[A]}{\mathrm{d}t} = \frac{1}{\sim 1400}\frac{-\mathrm{d}[\bigcirc]}{\mathrm{d}t}.$$

so

$$\text{A.3(a)}\quad \frac{1}{\sim 1400}\frac{-\mathrm{d}[\bigcirc]}{\mathrm{d}t} = k_1[A] + k_2[A]([A]_0-[A])$$

$$\text{A.3(b)}\quad \frac{-\mathrm{d}[\bigcirc]}{\mathrm{d}t} = \sim 1400\,[(k_1[A] + k_2[A]([A]_0-[A]))]$$

The key, now, is that each of the $Ir(0)_{\sim 300}$ catalyst active sites [B] produced is magnified effectively instantaneously (i.e., relative to its slower rate of production) and constantly by the catalytic reaction. This is most clearly illustrated by the *catalytic* reaction scheme shown below

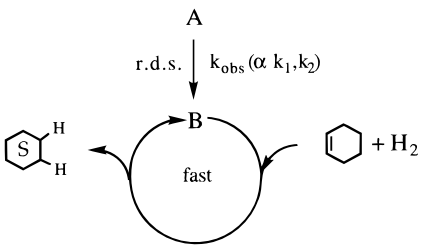

The key to obtaining a differential equation that is related to what we can follow, the

$$\frac{-\mathrm{d}[\bigcirc]}{\mathrm{d}t} = \frac{-\mathrm{d}[H_2]}{\mathrm{d}t}$$

is the magnification factor, eq A.4, and it is given by the stoichiometry of the pseudoelementary step. (Experimentally, this stoichiometry factor is best determined by the ratio [cyclohexene]/[cyclooctane] at the exact point all the [cyclohexene] is consumed.)

$$\text{A.4(a)}\quad [B]t = \frac{1}{1400}[\textcircled{S}]_t = \frac{1}{1400}([\bigcirc]_0 - [\bigcirc]_t)$$

by the mass balance equation,

$$[\textcircled{S}]_t = [\bigcirc]_0 - [\bigcirc]_t)$$

or, from $[B]_t = [A]_0 - [A]_t$ we obtain eq A.4b:

$$\text{A.4(b)}\quad [A]_0-[A]_t = \frac{1}{1400}([\bigcirc]_0 - [\bigcirc]_t)$$

Rearranging A.4b, and using the stoichiometry identity that

$$[A]_0 = \frac{1}{1400}([\bigcirc]_0$$

we obtain eq A.4c for $[A]_t$:

$$\text{A.4(c)}\quad [A]_t = [A]_0 - \frac{1}{1400}([\bigcirc]_0 - [\bigcirc]_t)$$

$$[A]_t = \frac{1}{1400}[\bigcirc]_t$$

Now, substituting A.4b and A.4c into eq A.3b (for$[A]_t$ and $[A]_0 - [A]_t$), yields eq A.5

$$\text{A.5}\quad \frac{-\mathrm{d}[\bigcirc]}{\mathrm{dt}} = k_1[\bigcirc]_t + \frac{k_2}{1400}[\bigcirc]_t([\bigcirc]_0 - [\bigcirc]_t)$$

This is differential form of the equation, A.5, that we use for the curvefits. Note that $k_{1(\text{curvefit})} = k_1$, but $k_{2(\text{curvefit})} = (k_2/1400)$ or $1400k_{2(\text{curvefit})} = k_2$.

Appendix B: Derivation of Eq 4

From eq A.1 (equals eq 3 in the text), and substituting for $[B] = [A]_0 - [A]$, one obtains the following equation which can be integrated and then evaluated at the indicated limits:

$$\frac{-\mathrm{d}[A]}{\mathrm{d}t} =$$

$$k_1[A] + k_2[A]([A]_0 - [A])\int_0^t \frac{-\mathrm{d}[A]}{[A](k_1 + k_2([A]_0 - [A]))} =$$

$$\mathrm{d}t\,\frac{1}{k_1 + k_2[A]_0} * \ln\left[\frac{k_1 + k_2([A]_0 - [A])}{[A]}\right]_0^t =$$

$$t\ln\left[\frac{(k_1 + k_2([A]_0 - [A]))[A]_0}{k_1[A]}\right] = (k_1 + k_2\,[A]_0)t$$

Expressing the resultant equation (above) in exponential form yields the desired eq 4

$$[A]_t = \frac{\frac{k_1}{k_2} + [A]_0}{1 + \frac{k_1}{k_2[A]_0} * \exp^{(k_1 + k_2[A]_0)t}}$$

Appendix C: Scaling Factor for the Rate Constant k_2

If one is to rigorously apply the autocatalytic model

$$A \xrightarrow{k_1} B \qquad \text{(C.1a)}$$

$$A + B \xrightarrow{k_2} 2B \qquad \text{(C.1b)}$$

where the sum reaction is

$$2A \rightarrow 2B \qquad \text{(C.1c)}$$

to the formation of nanoclusters

$$n\mathrm{Ir}(0) \rightarrow \mathrm{Ir}(0)_n \quad \text{(nucleation)} \qquad \text{(C.2a)}$$

$$\mathrm{Ir}(0) + \mathrm{Ir}(0)_n \rightarrow \mathrm{Ir}(0)_{n+1} \quad \text{(growth)} \qquad \text{(C.2b)}$$

one needs in fact to express eqs C.2(a,b) as in eqs C.3(a,b), since the catalytic species B corresponds to active surface atoms on the nanocluster:

$$n\mathrm{Ir(0)} \rightarrow \mathrm{Ir(0)}_{n(\text{surface atoms})} \quad \text{(C.3a)}$$

$$\mathrm{Ir(0)} + \mathrm{Ir(0)}_{n(\text{surface atoms})} \rightarrow \mathrm{Ir(0)}_{n+1(\text{surface atoms})} \quad \text{(C.3b)}$$

Let us now define $x_{(\text{nucleation or growth})}$ as the fraction of surface atoms gained in a reaction step (of nucleation or growth), eq C.4:

$$x_{(\text{nucleation or growth})} = \frac{\text{increase in no. of surface atoms}}{\text{increase in total no. of atoms}} \quad \text{(C.4)}$$

The autocatalysis model in eq C.1 can then be rewritten more precisely, for the present case of nanocluster formation, as eqs C.5a,b:

$$\mathrm{A} \xrightarrow{k_1} x_{\text{nucleation}}\mathrm{B} \quad \text{(C.5a)}$$

$$\mathrm{A} + x_{\text{nucleation}}\mathrm{B} \xrightarrow{k_2} (x_{\text{nucleation}} + x_{\text{growth}})\mathrm{B} \quad \text{(C.5b)}$$

where the sum reaction is

$$2\mathrm{A} \rightarrow (x_{\text{nucleation}} + x_{\text{growth}})\mathrm{B} \quad \text{(C.5c)}$$

At the end of the induction period, which also marks the end of the nucleation step (or at least most of it), less than 5% of the total amount of cyclooctane has evolved (see Figure 7 elsewhere),[20b] indicating that the nucleus size should be less than 15 atoms. In this size range, the value of $x_{(\text{nucleation or growth})}$ is ≥ 0.92.[46] Hence, we can approximate $x_{\text{nucleation}}$ as ≈ 1, from which we obtain

$$-\frac{1}{2}\frac{\mathrm{d[A]}}{\mathrm{d}t} = \frac{1}{1 + x_{\text{growth}}}\frac{\mathrm{d[B]}}{\mathrm{d}t} \quad \text{(C.6a)}$$

$$\frac{\mathrm{d[B]}}{\mathrm{d}t} = -\frac{1 + x_{\text{growth}}}{2}\frac{\mathrm{d[A]}}{\mathrm{d}t} \quad \text{(C.6b)}$$

$$[\mathrm{B}]_t = \frac{1 + x_{\text{growth}}}{2}([\mathrm{A}]_0 - [\mathrm{A}]_t) \quad \text{(C.6c)}$$

so that the rate equation becomes

$$-\frac{\mathrm{d[A]}}{\mathrm{d}t} = k_1[\mathrm{A}] + k_2[\mathrm{A}][\mathrm{B}] \quad \text{(C.7a)}$$

$$-\frac{\mathrm{d[A]}}{\mathrm{d}t} = k_1[\mathrm{A}] + k_2\frac{1 + x_{\text{growth}}}{2}[\mathrm{A}]([\mathrm{A}]_0 - [\mathrm{A}]_t) \quad \text{(C.7b)}$$

Hence, the value of k_2 obtained from curvefits is really $k_{2(\text{curvefit})} = k_2 x$, that is, it contains the scaling factor $x = (1 + x_{\text{growth}})/2$.

Supporting Information Available: Six lines of evidence against a particle-size-dependence alone as the explanation for the observed sigmoidal kinetic curves; the FORTRAN curve-fitting programs; Figures S-1−S-3 of the effects, respectively, of water, HOAc, and temperature on the sigmoidal hydrogenation curves; Figures S-4 and S-5 plotting the effects of, respectively, HOAc and temperature on the induction period and hydrogenation rates; Figures S-6−S-9 of selected TEM pictures and histograms of Ir(0) nanoclusters prepared, respectively, under Standard Conditions, with the addition of 1.4 equiv of polyoxoanion, and at 45 °C and at 10 °C; a tabulation of the prior literature of the mechanisms of colloid and nanocluster formation (24 pages). See any current masthead page for ordering and Internet access instructions.

JA9705102